UPPSALA
UNIVERSITET

Digital Comprehensive Summaries of Uppsala Dissertations from the Faculty of Science and Technology 720

Fundamental Properties of Functional Magnetic Materials

MAGNUS WIKBERG

ACTA
UNIVERSITATIS
UPSALIENSIS
UPPSALA
2010

ISSN 1651-6214
ISBN 978-91-554-7953-4
urn:nbn:se:uu:diva-133257

Dissertation presented at Uppsala University to be publicly examined in Polhemsalen, Ångströmlaboratoriet, Lägerhyddsvägen 1, Uppsala, Friday, December 17, 2010 at 09:15 for the degree of Doctor of Philosophy. The examination will be conducted in English.

Abstract
Wikberg, M. 2010. Fundamental Properties of Functional Magnetic Materials. acta universitatis upsaliensis. *Digital Comprehensive Summaries of Uppsala Dissertations from the Faculty of Science and Technology* 720. 72 pp. Uppsala. ISBN 978-91-554-7953-4.

Magnetic properties of powders, thin films and single crystals have been investigated using magnetometry methods. This thesis provides analysis and conclusions that are supported by the results obtained from spectroscopic and diffraction measurements as well as from theoretical calculations.

First, the magnetic behavior of transition metal (*TM*) doped ZnO with respect to doping, growth conditions and post annealing has been studied. Our findings indicate that the magnetic behavior stems from small clusters or precipitates of the dopant, with ferromagnetic or antiferromagnetic interactions. At the lowest dopant concentrations, the estimated cluster sizes are too small for high resolution imaging. Still, the clusters may be sufficiently large to generate a finite spontaneous magnetization even at room temperature and could easily be misinterpreted as an intrinsic ferromagnetic state of the *TM*:ZnO compound.

Second, influence of lattice strain on both magnetic moment and anisotropy has been investigated for epitaxial MnAs thin films grown on GaAs substrates. The obtained magnetic moments and anisotropy values are higher than for bulk MnAs. The enhanced values are caused by highly strained local areas that have a stronger dependence on the in-plane axis strain than out-of plane axis strain.

Finally, spin glass behavior in Li-layered oxides, used for battery applications, and a double perovskite material has been investigated. For both $Li(NiCoMn)O_2$ and $(Sr,La)MnWO_6$, a mixed-valence of one of the transition metal ions creates competing ferromagnetic and antiferromagnetic interactions resulting in a low temperature three-dimensional (3D) spin glass state. Additionally, $Li(NiCoMn)O_2$ with large cationic mixing exhibits a percolating ferrimagnetic spin order in the high temperature region and coexists with a two-dimensional (2D) frustrated spin state in the mid temperature region. This is one of the rare observations where a dimensional crossover from 2D to 3D spin frustration appears in a reentrant material.

Keywords: Magnetic anisotropy, magnetic aging, magnetic semiconductors, exchange interactions, magnetic oxides, spin glasses, lithium-ion batteries, short-range magnetic order

Magnus Wikberg, Faculty of Science and Technology, Box 256, Uppsala University, SE-75105 Uppsala, Sweden.

ISSN 1651-6214
ISBN 978-91-554-7953-4
urn:nbn:se:uu:diva-133257 (http://urn.kb.se/resolve?urn=urn:nbn:se:uu:diva-133257)

any turkey can measure magnetic properties,
the true insight is in knowing what sample to make

till mormor Solveig

List of Papers

This thesis is based on the following papers, which are referred to in the text by their Roman numerals.

I J. M. Wikberg, R. Knut, S. Bhandary, I. di Marco, M. Ottosson, J. Sadowski, B. Sanyal, P. Palmgren, C. W. Tai, O. Eriksson, O. Karis and P. Svedlindh
Magnetocrystalline anisotropy and uniaxiality of MnAs/GaAs(100) films
Phys. Rev. B, in peer review (2010) .

II J. M. Wikberg, R. Knut, A. Audren, M. Ottosson, M.K. Linnarsson, O. Karis, P. Svedlindh and A. Hallén
Annealing effects on structural and magnetic properties of Co implanted ZnO single crystals
J. Appl. Phys, submitted (2010)

III R. Knut, J. M. Wikberg, K. Lashgari, V. A. Coleman, G. Westin, O. Karis, and P. Svedlindh
Magnetic and electronic characterization of highly Co doped ZnO: An annealing study at the solubility limit
Phys. Rev. B, **82** 094438 (2010)

IV D. Iuşan, R. Knut, B. Sanyal, O. Karis, O. Eriksson, V. A. Coleman, G. Westin, J. M. Wikberg and P. Svedlindh
Electronic structure and chemical and magnetic interactions in ZnO doped with Co and Al: Experiments and ab initio density-functional calculations
Phys. Rev. B, **78** 085319 (2008)

V J. M. Wikberg, M. Dahbi, I. Saadoune, T. Gustafsson, K. Edström and P. Svedlindh
Magnetic order, aging and spin frustration in a percolating spin system, $LiNi_{0.8}Co_{0.1}Mn_{0.1}O_2$
J. Appl. Phys., **180** 083909 (2010)

VI J. M. Wikberg, M. Dahbi I. Saadoune T. Gustafsson K. Edström and P. Svedlindh
Dimensionality crossover and frustrated spin dynamics on a triangular lattice
Phys. Rev. B, **81** 224411 (2010)

VII M. Dahbi, J. M. Wikberg, I. Saadoune, T. Gustafsson, P. Svedlindh and K. Edström
A delithiated $LiNi_{0.65}Co_{0.25}Mn_{0.10}O_2$ electrode material: a structural, magnetic and electrochemical study
Electrochimica Acta, **54**, 3211 (2009)

VIII I. Saadoune, M. Dahbi, M. Wikberg, T. Gustafsson, P. Svedlindh and K. Edström
Effect of the synthesis temperature on the structure and electrochemical behavior of the $LiNi_{0.65}Co_{0.25}Mn_{0.10}O_2$ positive electrode material
Solid State Ionics **178**, 1668 (2008)

IX A.K. Azad, J. M. Wikberg, S.-G. Eriksson, A. Khan and P. Svedlindh
Spin-glass transition in a La-doped Sr_2MnWO_6 double perovskite
Phys. Rev. B, **77** 064418 (2008)

Reprints were made with permission from the publishers.

Contents

List of abbreviations and terms

AC	alternating current
AC/DC	Australian rock band, formed in Sydney 1973
AF	antiferromagnetic
c	speed of light, = 2.9979×10^{8} m/s
DC	direct current
eV	electron volt, = 1.60219×10^{-19} J
ε_o	permemittivity of free space, = 8.85419×10^{-12} F/m
FC	field cooled
FM	ferromagnetic
$\hbar$	Planck's constant, = $h/2\pi$ = 1.05459×10^{-34} Js
k_B	Boltzmanns constant, = 1.3807×10^{-23} J/K
k_F	Fermi wave vector
M	magnetization
$m_{ZFC}(t)$	zero field cooled magnetic relaxation
μ_B	Bohr magneton, = 0.92741×10^{-23} J/T or A·m^2
μ_{eff}	effective magnetic moment
μ_o	permeability of free space, = $4\pi\times10^{-7}$ Vs/Am
Oe	Oersted, = $10^3/4\pi$ A/m
T_c	Curie temperature
T_g	glass temperature
T_m	measuring temperature
T_N	Néel temperature
T_r	temperature of irreversibility
θ_w	Weiss temperature
χ	susceptibility
χ'	in-phase susceptibility
χ''	out-of-phase susceptibility
χ_{FC}	field cooled susceptibility
χ_{ZFC}	zero field cooled susceptibility
ZFC	zero field cooled
Å	Ångström, = 10^{-10} m

1. Introduction

From the observations of attraction between iron and magnetite to mapping of human brain activity, magnetism has enchanted curious humans for millenniums. This macroscopic phenomenon that holds important messages on refrigerator doors has a quantum mechanical description where the magnetic moment arises from the electron spin and motion around the atom. A true scientific explanation of magnetism is not possible, yet it is the simplest proof of quantum physics and relativity.

The word magnet is believed to originate from the ancient Greek tribe *The Magnetes* who lived in Magnesia, which is an area with large amounts of naturally occurring magnetic ore of the iron oxide, magnetite. Magnetite (Fe_3O_4) was used in the first compasses and was given the name "lodestone"which is old English for lead- or "waystone". The first known statements of magnetism date back to *Thales of Miletus* (634 - 546 BC). In 1600, William Gillbert published a detailed study of magnetism where he proposed that even Earth itself was a giant magnet [1]. The world of magnetism was changed in 1820 when Hans Christian Ørstedt presented his findings about how a circular magnetic field is produced when an electric current flows through a wire. It was then that the field of electromagnetism was born. Some years later in 1865, the most significant discovery of the 19th century [2] was presented; the Maxwell equations:

$$\nabla \cdot \mathbf{E} = \frac{\rho}{\varepsilon_o}, \quad \nabla \cdot \mathbf{B} = 0, \quad \nabla \times \mathbf{E} = -\partial \mathbf{B}/\partial t, \quad \nabla \times \mathbf{B} = \mu_o \mathbf{J} + \mu_o \varepsilon_o \partial \mathbf{E}/\partial t,$$

relating the electric field (**E**) with the magnetic field (**B**). James Clerk Maxwell concluded that light was an electromagnetic wave and established the connection between magnetism and light ($c = 1/\sqrt{\varepsilon_o \mu_o}$). In 1906, Pierre Weiss presented the molecular field theory which explains the earlier observations made by Pierre Curie of a transition temperature for the ferromagnetic state, the Curie temperature (T_c). Weiss proposed that a molecular field acts in a ferromagnetic material magnetizing it to saturation and consequently the material is "spontaneously magnetized". He claimed that this was valid below and even (incorrectly) above T_c explaining that above T_c the ferromagnet was divided in to small regions, or domains, organized in such a way that the net magnetization became zero. It was later established that Weiss' two postulates of *i*) spontaneous magnetization and *ii*) formation of domains, are correct. The development of atomic theory during the 20th century along with the dis-

covery of the electron and its dual nature (spin up and/or spin down) and the advancement of relativity and quantum mechanics have determined the understanding of the magnetic phenomenon as we know it today.

This thesis includes results from magnetic measurements performed mainly at the division of Solid State Physics at Uppsala University. The magnetic properties of Co:ZnO, MnAs, (Sr,La)$MnWO_6$ and Li(NiCoMn)O_2 have mainly been investigated through superconducting quantum interference device (SQUID) magnetometry. The interpretation of the measured magnetic behavior was assisted by results obtained from spectroscopy and diffraction methods as well as theory, in part or mainly performed by others. First, an overview will be given of the fundamentals of interaction, anisotropy and spin frustration in magnetic materials. This is followed by two separate sections with results and discussion of Spintronic materials (Co:ZnO, and MnAs) and frustrated oxides ((Sr,La)$MnWO_6$ and Li(NiCoMn)O_2).

1.1 Fundamentals

What!? How can people use something they don't understand?.....
It's easy! People do it every day – it's called the iPhone. [1]

Consider a substance with randomly oriented magnetic moments or spins as seen in the left panel of Fig. 1.1a. If subjected to a magnetic field the resulting magnetic susceptibility is either positive (paramagnetic) or negative (diamagnetic). In fact, all substances, if not magnetically ordered, are either para- or diamagnetic which is why it is possible to levitate a frog [3] (and consequently a human being) with a high enough magnetic field. If the magnetic moments in the substance will order below some temperature it is either ferromagnetic with all magnetic moments aligned along a common direction, cf. Fig. 1.1b, antiferromagnetic with oppositely aligned magnetic moments as in Fig. 1.1c or ferrimagnetic where the moments have opposite alignment but differ in magnitude as in Fig. 1.1d.

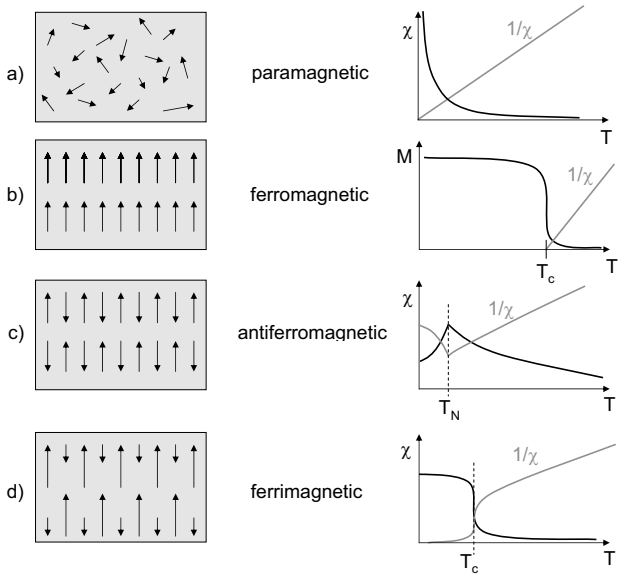

Figure 1.1: Schematic view of different spin states and the corresponding temperature dependence of the susceptibility (χ, black) and inverse susceptibility ($1/\chi$, grey).

In order to determine the spin order of a substance one can write the exchange interaction between two electrons in terms of their spin momenta by using the Hamiltonian proposed by Werner Heisenberg (H_J),

$$H_J = \sum_{i,j} J_{ij} \mathbf{S}_i \mathbf{S}_j, \tag{1.1}$$

[1] V. J. Sternhagen

where J_{ij} is the exchange coupling constant between the spins $\mathbf{S}_i$ and $\mathbf{S}_j$. The magnetic properties are dependent on the sign and magnitude of the interactions between the spins. $J_{ij}>0$ implies ferromagnetic interactions between the spins, while $J_{ij}<0$ corresponds to antiferromagnetic interactions. The question is what determines the sign of J_{ij}, i.e. the type of interactions present in a compound?

1.1.1 Magnetic Interactions

The energy difference between the FM and AF state defines J_{ij}(=[E_{AF}-E_{FM}]/2). An AF (↑↓) spin structure is constrained by the Pauli principle which forbids occupancy of parallel spins in 'bonding' states. A FM (↑↑) spin structure is a many electron effect implying that some electrons occupy excited one-electron states gaining the necessary energy from Coulomb repulsion between electrons, thus punishing ↑↓ configurations in one electron orbitals. Hence, J_{ij} depends on the number of electrons as well as on the inter atomic distance.

In transition metal (TM) magnets the orbital moment is suppressed by the crystal lattice, i.e. quenched by the crystal field. Thus the orbital magnetic moment can be neglected when estimating the total magnetic moment. In most TM-oxides the magnetic moment is defined by the number of unpaired spins ($2\mu_B\mathbf{S}$). The exchange interaction between TM-ions is in general determined by overlap between electron orbitals. Indirect exchange interaction between TM-cations is in most cases created by the $2p$ electrons of the O^{-2} anion. *Superexchange interaction* implies localized electrons remaining in their respective orbitals while the spin-spin interaction is mediated by the $2p$-electrons, as seen in Fig. 1.2a displaying an AF superexchange. The sign of the interaction depends on the $TM-O$ orbital overlap and the bond angle $TM-O-TM$ and can be predicted by the so-called *Goodenough-Kanamori* rules [4, 5]. In case of *double exchange interaction* an electron transfer occurs from the $2p$ O^{-2} to one cation, which is simultaneously replaced by a 3d electron from the other cation, as seen in Fig. 1.2b, leading to FM interactions due to strong on-site Hund's coupling. In the case of magnetic impurities in a non-magnetic metallic host material, the interactions between the impurities, where the conduction electrons play a similar role as $2p$ electrons in oxides, are described by the *Ruderman-Kittel-Kasuya-Yoshida* (RKKY) interactions. Imagine throwing a stone in the water and the resulting wave. This is how the magnetic moment creates a wave-like perturbation in the sea of conduction electrons yielding magnetic interactions described by:

$$J(R) = J_o \frac{2k_F R cos(2k_F R) - sin(2k_F R)}{(2k_F R)^4}, \tag{1.2}$$

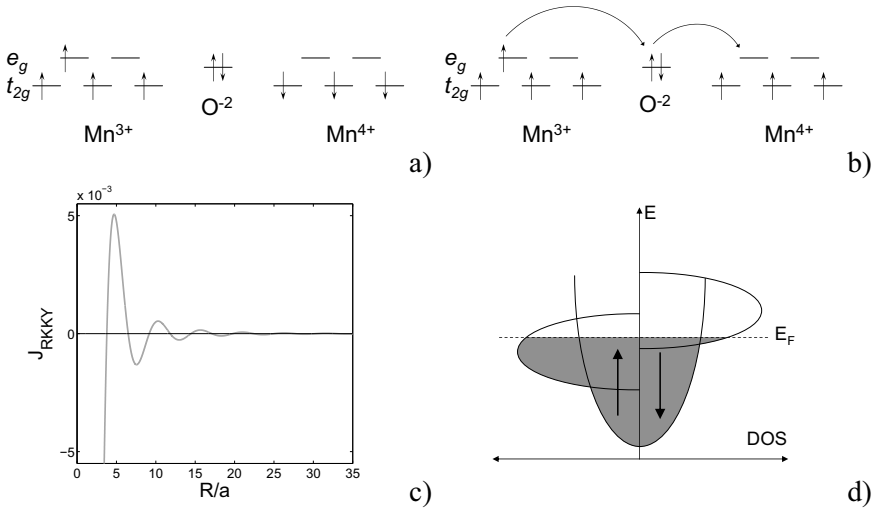

Figure 1.2: Schematic view of **a)** superexchange interactions, **b)** double exchange interactions, **c)** RKKY interactions with the separation (R) normalized with the atomic radius (a) for Mn atoms and **d)** itinerant magnetism.

where k_F is the Fermi wave vector and R is the distance between the magnetic impurities. The surprising result is that, in addition to the strength, the sign of the interaction also varies with the distance between magnetic impurities, cf. Fig. 1.2c. RKKY like behavior can be found in alloys, spin glasses and even dilute magnetic semiconductors (DMS).

Materials with delocalized electrons such as Fe, Ni and Co exhibit *itinerant* magnetism. Simply put, in itinerant materials the atomic orbitals hybridize and form energy bands where the quantum state is defined by a wave vector and the electron spin. The delocalized states are filled with electrons until the Fermi level is reached. For FM materials the density of states (DOS) for spin-up (majority) electrons contains more electrons than for spin-down (minority) electrons as seen in Fig. 1.2d, and thus, a ferromagnetic state is formed. Itinerant magnets with half-filled bands show a strong tendency to form an AF state since the hybridization energy for half-filled spin-up and spin-down bands is lower than for a completely filled spin-up band.

1.1.2 Magnetic Anisotropy

The direction of the spontaneous magnetization of a specimen is determined by its magnetic anisotropy. If the field is applied along the *hard*-axis of magnetization, seen in Fig. 1.3, the energy necessary to rotate the spin system of a domain away from its *easy*-axis and to saturate the magnetization along the field direction is called the anisotropic energy (E_a). Magnetocrystalline

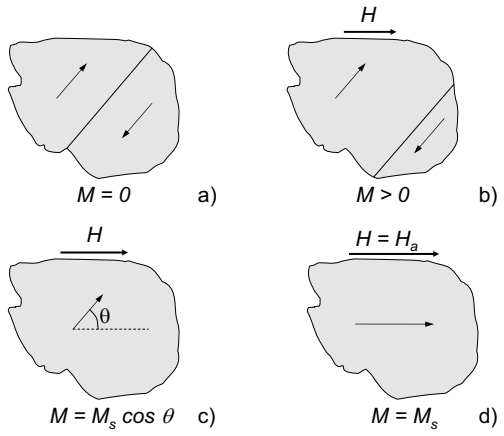

Figure 1.3: Schematic view of the magnetization process in a ferromagnet.

anisotropy (MCA) is an intrinsic magnetic anisotropy and is mainly due to the coupling between the spin and the orbital motion of the electron in the crystal lattice. The measured E_a is therefore (only) the energy required to overcome the spin-orbit coupling since:

i) spin-spin coupling is very strong and acts to keep neighboring spins in a parallel or anti parallel configuration. The exchange energy is isotropic and only dependent on the adjacent spin angle, and the spin axis is not related to the crystal lattice.

ii) lattice-orbit coupling is strong with the orientation strongly fixed to the lattice due to crystal field quenching of the orbital moment.

The most simple case of MCA is uniaxial anisotropy which is valid for a crystal with a single *easy*-axis along which the magnetization can point either up or down. A generalized expression for the anisotropic energy density (F) in case of uniaxial anisotropy is given by:

$$F = \sum_i K_i \sin^{2i} \theta, \tag{1.3}$$

where the anisotropy constants, K_i, describe the strength of the anisotropy and θ is the angle between the magnetization and the anisotropy axis. In most cases it is sufficient to only consider the first 3 terms where K_0 is ignored since

it is independent of the magnetization orientation/angle. If $K_1 > 0$ the material is said to have an *easy-axis*, while if $K_1 < 0$ and $K_2 < 0$ or if $K_1 < 0$ and $K_2 < -K_1/2$ the material has an *easy-plane* of magnetization. If $K_1 < 0$ and $K_2 > -K_1/2$, there is an *easy-cone* of magnetization. For example, hcp-Co exhibits $K_1 = 4.5 \times 10^5$ J/m^3 and $K_2 = 1.5 \times 10^5$ J/m^3, i.e. *easy-axis* MCA. The field required to saturate a sample along its *hard*-axis is called the anisotropy field (H_a) and is defined as $H_a = 2K_1/\mu_o M_s$. The anisotropy constants can

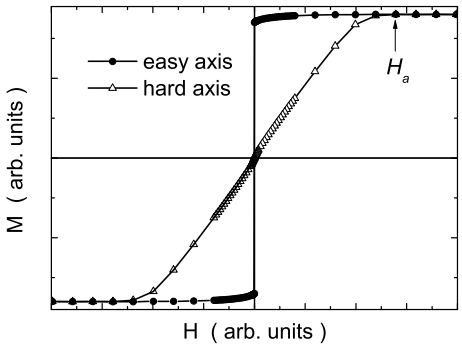

Figure 1.4: Magnetization (M) versus field (H) of a hexagonal compound measured along its *easy* (red circles) and *hard* (blue triangles) axis of magnetization.

be determined through various methods such as torque magnetometry, ferromagnetic resonance and magnetization versus field measurement using either the area or curve fitting method. In the curve fitting method a theoretical expression for the magnetization curve is fitted to the experimental results. In this work a curve fitting method has been employed. First, one must set up the expression for the relevant total energy density. In our case, it is the energy density corresponding to the hard axis magnetization curve,

$$F = \frac{E_a}{V} = K_1 \sin^2\theta + K_2 \sin^4\theta - \mu_o H M_s \cos\theta, \tag{1.4}$$

where θ is the angle between the magnetization and the anisotropy axis, and $-\mu_o H M_s \cos\theta$ is the Zeeman term. The Zeeman term (or energy) describes the interaction of a magnetic moment with an applied magnetic field [6] and implies that the magnetic moment will try to reduce its energy by aligning itself parallelly with the applied magnetic field. The energy minimum is given by $\frac{\partial}{\partial\theta}F = 0$ and through the relation $M = M_s \; cos \; \theta$ an expression for the applied field as a function of the magnetization is obtained:

$$H = -\frac{1}{\mu_0 M_s}\left\{2K_1 + 4K_2\left[1 - \left(\frac{M}{M_s}\right)^2\right]\right\}\frac{M}{M_s}, \tag{1.5}$$

which is fitted to the experimental results for the hard-axis magnetization yielding the K_i-values. When evaluating K_1, the shape anisotropy (K_{sh}) must be considered in some cases. Shape anisotropy arises because the demagnetizing field (H_d) is larger along a short axis than along a long axis of a sample geometry; thus, a larger field is necessary to obtain the same magnetization when applying the field along the short axis. The shape anisotropy energy can be derived from the magnetostatic self-energy, which in case of a homogeneous magnetization is given by

$$E_{ms}/V = -\frac{\mu_o}{2}\mathbf{M}\cdot\mathbf{H}_d\,, \tag{1.6}$$

where $\mathbf{H}_d = -N_d\mathbf{M}$. For plate like magnets, with a demagnetizing factor $N_d = 1$ perpendicular to the plate surface and $N_d = 0$ in the plane of the plate, the magnetic field, H_s, necessary to saturate the magnetization perpendicular to the plate is related to the shape-anisotropy field, $-2K_{sh}/\mu_0 M_s$. Since H_s=$N_d M_s$, K_{sh} for thin films is given by:

$$K_{sh} = -\frac{\mu_o M_s^2}{2}. \tag{1.7}$$

Magnetic anisotropy could also arise from stress, annealing in a magnetic field and/or plastic deformation, but since no such cases are addressed in this thesis they will not be considered further.

1.1.3 Magnetic Frustration

A magnetically frustrated state arises in a spin system because all the exchange interactions cannot be satisfied simultaneously. In Fig. 1.5b, a bond disordered system is illustrated, but a frustrated spin system may also arise from site disorder implying randomness in the spin positions. Since the spins have a glassy structure, these materials are referred to as *Spin Glasses* (SG).

Another interesting phenomenon is the so-called reentrant spin glass (RSG). These materials experience a magnetic ordering of FM (T_c) or AF (T_N) type and upon further cooling a transition to a frustrated spin state occurs and is referred to as the reentrant spin glass transition (T_{RSG}). RSGs posses many of the characteristics of SG systems (e.g. slow spin dynamics and magnetic aging) but are more sensitive to an applied field due to the coupling between the field and the order parameter. In a frustrated

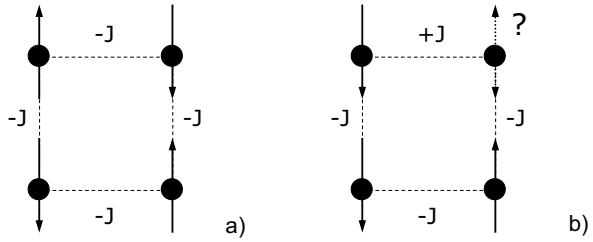

Figure 1.5: Illustration of a magnetically **a)** ordered and **b)** frustrated state. The frustrated state in **b)** is due to bond disorder.

spin system, the magnetization exhibits a strong time dependence with a relaxation that extends beyond experimentally accessible time scales. An archetypical spin glass shows a cusp in the zero field cooled (ZFC) as well as a divergence between the field cooled (FC) and the ZFC curves. In Fig. 1.6, results from AC susceptibility measurements are shown with a clear dependence of the AC field frequency (f) in both the in-phase (χ') and out-of-phase (χ'') components of the susceptibility.

The frequency dependence of χ' or χ'' can be analyzed by dynamic scaling. For an ordinary three dimensional (3D) spin glass material, one can assume critical slowing down of the spin dymanics. The relaxation time ($\tau = 1/2\pi f$) is related to the correlation length through $\xi \sim \left|(T - T_g)/T_g\right|^{-\nu}$. The relation $\tau \sim \xi^z$ implies that τ should diverge when approaching the spin glass temperature, T_g, from above according to:

$$\tau(T_f) = \tau_o \varepsilon^{-z\nu}, \tag{1.8}$$

where $\varepsilon = (T_f - T_g)/T_g$ and T_f is the spin freezing temperature. Typical values of the critical exponent, $z\nu$, is 8-10 and the atomic spin flip time, τ_o, $\simeq 10^{-13}$ s [7] for 3D spin glasses. If the frequency dependence of the magni-

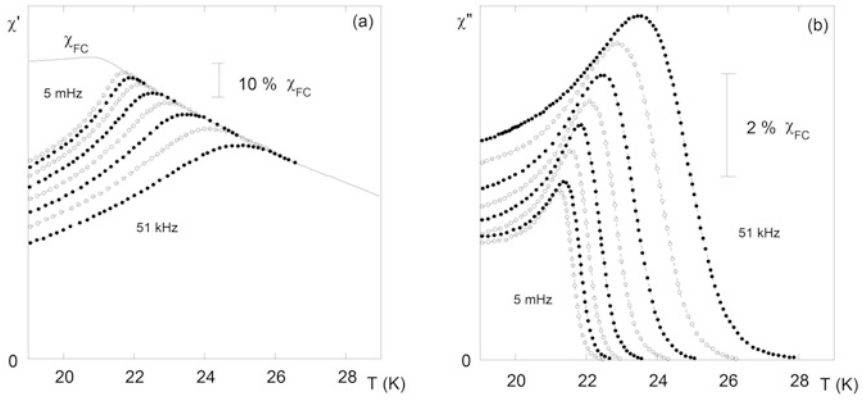

Figure 1.6: Archetypical AC susceptibility results for an Ising spin glass, $FeMnTiO_3$, for frequencies between 5×10^{-3} to 51×10^{3} *Hz* with **a)** in-phase susceptibility (χ') and **b)** out-of-phase susceptibility (χ'').

tude of χ'' is reversed, i.e. the lowest f yields the highest χ'', it could indicate a frustrated spin state in two dimensions (2D) [8]. Since the correlation length only diverges at zero temperature for a 2D spin glass system, there is no phase transition at finite temperature [9]. The dynamics is governed by thermal excitations over energy barriers; thus, with a $T_g \rightarrow 0$ the behavior follows a generalized Arrhenius law [10]:

$$ln(\tau/\tau_{o2}) \propto \frac{1}{T}\xi^{\psi} \propto T_f^{-(1+\psi\nu)}, \tag{1.9}$$

where ψ is the energy barrier exponent with a typical value of $\psi\nu>1$ for 2D spin glasses [11]. If $\psi\nu=0$, the system is governed by thermally activated dynamics [12] as in superparamagnetic systems.

Magnetic aging, which can be investigated through magnetic relaxation measurements, is an inherent property of spin glass materials. Magnetic relaxation behavior is very sensitive to the temperature and applied magnetic field measurement history below T_g. To perform relaxation measurements, the sample is cooled in zero field to the measurement temperature (T_m) and kept constant at T_m for a wait time (t_w). Subsequently, a small field H_{dc} is applied and the magnetic relaxation ($m_{ZFC}(t)$) is recorded. A common way to analyze $m_{ZFC}(t)$ is by utilizing the relationship to the ZFC relaxation rate [$S(t)$]:

$$S(t) = \frac{1}{H_{dc}}\frac{\partial m_{ZFC}}{\partial \ln(t)}. \tag{1.10}$$

The most striking feature of the $S(t)$-curve is that a maximum relaxation rate ($S_{\max}$) exists (that is an inflection point in $m_{ZFC}(t)$) at an observation time (t) related to t_w. For ordinary spin glasses $S_{\max}$ occurs at $t\approx t_w$. At $t\approx t_w$, non-

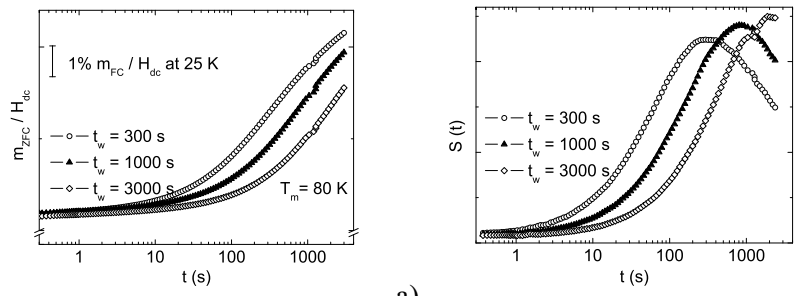

Figure 1.7: Magnetic aging with **a)** magnetic relaxation $m_{\mathrm{ZFC}}(t)$ versus t and **b)** relaxation rate $S(t)$ versus t.

equilibrium magnetization dynamics are examined while for $t \ll t_w$ a quasi-equilibrium dynamic process is examined although the spin glass compound as a whole is still in a non-equilibrium state [13]. Temperature cycling relaxation rate experiments have also been performed within this thesis work. After a wait time t_w at T_m, the sample is subjected to a temperature increase or decrease to $T_m \pm \Delta T$ and held there for a second wait time (t_{w2}), for this thesis t_{w2}=100 s, and subsequently brought back to T_m before applying H_{dc} and commencing the relaxation measurement. If S_{max} occurs at $t \ll t_w$, or if

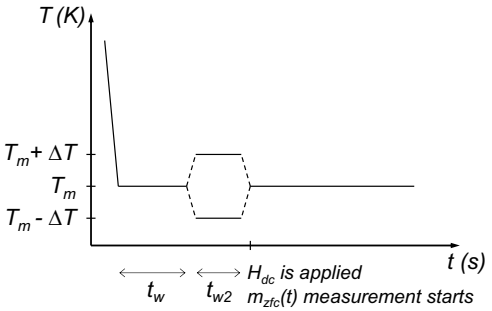

Figure 1.8: Schematic view of a cycling experiment.

two maxima are observed in the $S(t)$-curve with one occurring at $t \ll t_w$, the spin system is said to be fully or partly reinitialized. The occurrence of reinitialization, irrespective of the sign of ΔT, is a signature of a reentrant spin glass material above the spin glass temperature but below the spin ordering temperature T_c or T_N. When the temperature cycling experiment is performed for a T_m below T_g, reinitialization occurs for only positive (not negative) temperature cycles at comparable t_{w2} wait times [14].

2. Spintronic Materials

Predictions of Moore's law[1] [15] failing in 15 to 20 years have created an interest in spin transport electronics - Spintronics - due to their potential to push forward the breakdown of Moore's law. Despite that the word *Spintronics* was created[2] in 1996 within the DARPA initiative *Magnetic Materials and Devices* [16], the research impinges on diverse areas in physics such as magnetism, semiconductivity and optics [17]. In *Spintronics*, the microelectronic device relies on the spin of the electron for memory and to carry the information. This opens a new generation of spin-dependent devices that make use of effects arising from the interaction between magnetic material properties and carrier spin. By adding the spin degree of freedom (or using it alone), the capability and performance in electronic products will substantially increase [18]. These gains arise from the potential increased data processing speed, decreased power consumption, nonvolatility and increased integration densities compared with today's semiconductor devices.

The use of Spintronics in today's commercial devices is mainly connected to spin valves in magnetic hard disk drives. Spin valves are based on the giant magnetoresistance (GMR) effect which was discovered in 1988 by both Albert Fert [19] and Peter Grünberg [20] independently of each other. Each were awarded the Nobel Price in Physics in 2007. A GMR device operates by two ferromagnetic (FM) layers being separated by a nonferromagnetic metal spacer of nanometer thickness. When the magnetizations of the FM layers are in parallel the spin valve is open, the device exhibits a low resistance. When the FM layers have antiparallel orientation the spin valve is closed, the device has high resistance. Usually, one of the FM layers is static (or pinned) while the orientation of the second layer is controlled with a small magnetic field. Even though GMR spin valves lead to a dramatic increase in the area storage density in hard disk drives, the era of GMR is already antiquated and, after only ten years, has been replaced by spin dependent tunneling devices. A magnetic tunnel junction (MTJ) uses a non metallic spacer and may exhibit a magnetoresistive effect surpassing that of the GMR device by a factor of ten at room temperature [21].

---

[1] the number of transistors on a chip doubles every 24 months

[2] *Since the project title "Magnetic Materials and Devices" did not reflect the efforts involved, one of us (SW) proposed that the project be renamed "Spintronics", which was an acronym for SPIN TRansport electrONICS;* S.A. Wolf [16]

The Datta-Das proposal of the spin field effect transistor (SFET) [22] is a more novel approach regarding electron spin control during charge transport and the use of it as an information carrier. The SFET has a symmetry resembling that of an ordinary FET, shown schematically in Fig. 2.1, where a current injected by the source is allowed to flow (*ON*) or not to flow (*OFF*) by controlling the gate voltage. A SFET uses an available semiconductor material, in this case a two dimensional electron gas (2DEG), and FM contact materials as source and drain. The source injects a spin polarized current into the 2DEG which is then detected by the drain. The device is *ON* if the spins align parallely to the spins in the drain; otherwise, the device is *OFF*. The gate voltage is used to generate a fictitious magnetic field controlling the precession of the electron spin and determines if the electrons arrive to the drain as parallel or antiparallel (or anything in between) spins [17]. The challenge for this type of device is to find a material that would give a highly spin-polarized electrical current. One proposal is to use ohmic injection of electrons through a FM metal since the conductivity of the majority spin electrons (spin-up electrons) differs substantially from that of the minority spin electrons (spin-down electrons).

Dilute magnetic semiconductors (DMS) have been proposed for use as FM contacts since the creation of an ohmic metal-semiconductor contact involves heavily doping the semiconductor surface in order to lower the Schottky-barrier. This will in turn lead to spin-flip scattering and hence loss of spin-polarization [18]. Even though magnetic materials have been used in the data storage industry since the 1950's [3], the beginning of the *Spintronic* era is commonly set to the discovery of the GMR-effect.

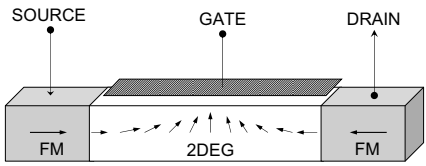

Figure 2.1: Datta-Das proposal of a spin FET with a two dimensional electron gas (2DEG) and ferromagnetic (FM) contacts (source and drain) and a gate controlling the precession of the electron spins

[3] IBM 737, Magnetic core storage unit launched 1954

2.1 Dilute Magnetic Semiconductors

absence of evidence is not evidence of absence[4]

The subject of dilute magnetic semiconductors (DMS) has emerged from the idea that impurity doping of ordinary semiconductors changes the material properties such as altering the band gap or making them *n*- or *p*-type. It has been proposed that non-magnetic semiconductors become magnetic by introducing a small amount of magnetic elements, and, hence, are named *dilute* magnetic semiconductors. One example of a successfully fabricated DMS material is the III-V[5] semiconductor, GaAs doped with Mn. (Ga,Mn)As was discovered in 1996 and, at that time, a T_c= 60 K [23] was reported. Recently though, a $T_c \approx$ 180 K [24] has been achieved.

The Zener model has successfully been used to predict magnetic properties in (Ga,Mn)As. In 2000 Dietl *et al.* employed the Zener model to predict T_c in various DMS materials and indicated that wide-band gap materials such as GaN and ZnO doped with Mn could yield a T_c above room temperature [25]. These and similar predictions have triggered a tremendous research effort, both experimentally and theoretically, on wide-band gap DMS materials. Despite initial intriguing experimental reports of T_c's exceeding room temperature, no group has yet shown reproducible results of intrinsic ferromagnetism above room temperature. One problem to achieve room temperature ferromagnetism in ZnO is the difficulty to produce *p*-doped ZnO with the very high hole concentration ($\sim 3.5 \times 10^{20}$ holes per cm^3 [25]) necessary for hole induced ferromagnetism, as predicted by Dietl *et al*. If, however, the obstacles could be overcome, DMS ZnO would be the ultimate multifunctional material enabling combinations of optical, semiconducting, mechanical and magnetic properties and having applications in optoelectronics [26] and quantum computing [27].

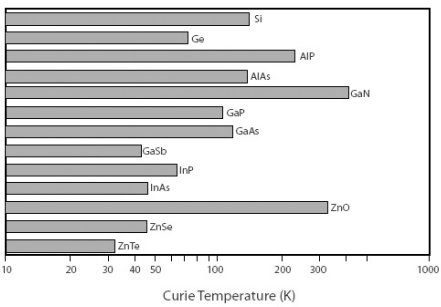

Figure 2.2: Predicted magnetic ordering temperatures of *p*-type materials with a doping concentration of 5% Mn and 3.5×10^{20} holes per cm^3. After Dietl *et al.* [25]

[4] D.D. Sarma

[5] read: three-five's, the roman III and V relate to their respective column in the periodic table

2.1.1 Transition metal doped ZnO

Zinc oxide is a transparent semiconductor with a direct band gap of 3.4 eV and normally forms a hexagonal (wurtzite) crystal structure with a_{hex}= 3.25 Å and c_{hex}= 5.21 Å [28]. Interest in ZnO is due to its piezoelectric properties and the possibility to use it in UV-light emitters, gas-sensors and high power electronics. It is relatively simple to *n*-dope ZnO with either Al, Ga, In or an excess of Zn. ZnO displays a substantial resistance to the formation of shallow acceptor levels making *p*-type doping difficult to achieve [29].

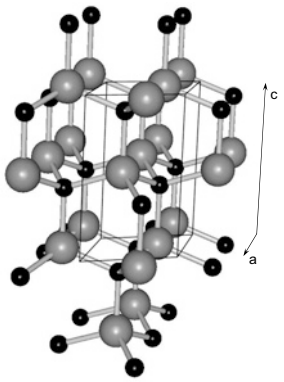

Figure 2.3: ZnO in its hexagonal wurtzite structure with Zn and O represented by grey and black balls, respectively (created with VESTA [30]).

The ability to substitutionally replace Zn^{2+} with a cation at elevated temperatures has been known for a long time [31]. The first report on experiments seeking ferromagnetism in TM doped ZnO is only a bit more than a decade old [32]. Despite initial reports presenting no evidence of long range magnetic order and stating that the magnetic coupling between the Mn ions in ZnO is of short range antiferromagnetic type [33], in 2003, Sharma *et al.* claimed to have produced ferromagnetic thin films of $Zn_{1-x}Mn_xO$ with x≈0.02, and M_s= 0.16 μ_B per Mn atom [34]. This publication ignited such hype around Mn:ZnO that even the principal of KTH claimed that "this is the biggest discovery since the transistor"[35]. Their reported magnetic moment at room temperature was very small; the magnetic moment is equivalent to 70μg of $MnFe_2O_4$. Thus, a very small amount of ferrite nanoparticles (untraceable in XRD) could give rise to the observed room temperature ferromagnetism [36]. This, as well as other possible scenarios, are historically neglected by authors claiming ferromagnetism in *TM*-doped ZnO.

We have also performed a study on ZnO doped with a nominal concentration of 5 at-% Mn. The samples were prepared by magnetron sputtering on Si substrates in the presence of either Ar or N_2 gas and, in certain cases, a cyclotron plasma source was used to enhance the incorporation of N in the samples. The idea sprung from the prediction that Zn vacancies, acting as acceptor

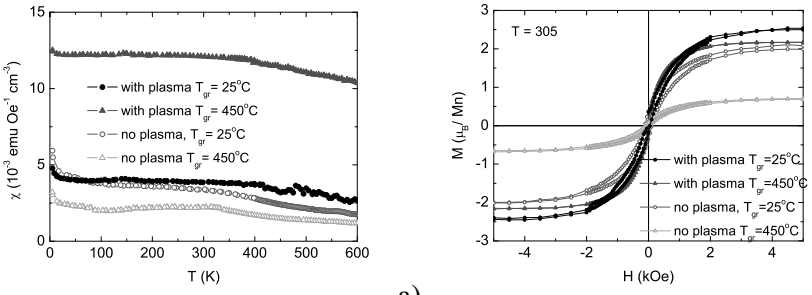

a) b)

Figure 2.4: Results from VSM measurements. Samples were grown at (T_{gr}) 25° or 450°C (circles or triangles), filled symbols are samples grown with a N-plasma source and open symbols are without this source. **a)** susceptibility (χ) versus temperature (T) (applied field between 10 and 350 K was 2 kOe and between 300 and 700 K 4 kOe). **b)** shows magnetization (M) versus field (H) at 305 K.

defects, will change the ground state from antiferromagnetic to ferromagnetic [37]. Additionally, acceptor defects and hence a ferromagnetic ground state could also be achieved through incorporation of nitrogen in the film. The results, shown in Fig. 2.4, indicate a very strong magnetization at room temperature (much stronger than that obtained by Sharma *et al.*) with a clear hysterisis in the *M vs H* curve. From these results, it is obvious that the large magnetic moment measured is partially caused by using a N-plasma source during film deposition, though the largest effect seems to originate from the low temperature growth. The question of what casuses the observed behavior arises?
X-ray magnetic circular dichroism (XMCD) measurements (not shown) were performed at MAX-Lab in Lund as well as at ESRF in Grenoble. The magnetic field was applied in-plane during measurements and reveal no dichroism; hence, there is no ferromagnetism due to Mn interactions. Since an XMCD measurement only probes the first few nanometers into a sample (<10 nm), a possible explanation of the observed ferromagnetism could be that the FM moments are buried deep in the sample. To investigate the depth distribution of Mn, we also made secondary ion mass spectroscopy (SIMS) measurements. The SIMS results (not shown) showed no concentration increase of Mn when approaching the film/substrate interface, but rather a homogeneous distribution of Mn in the samples. From energy-dispersive x-ray (EDX) analysis it was concluded that the samples grown at room temperature, with and without a plasma source, had a Mn content of 2.4 and 1.4 at-% as well as a N content of 5.6 and 5.4 at-%, respectively. The corresponding result for films grown at 450°C was 4.4 and 4.6 at-% Mn as well as 5.8 and 5.3 at-% N. The plasma source only seems to have a minor influence on the N content, and the only safe statement based on these results would be that it affects the Mn concentration for film growth performed at RT. XRD measurements reveal

several unknown diffraction peaks not related to ZnO as well as an indication of Mn_3O_4 in all samples. The saturation magnetization (M_s) measured at 10, 305 and 500 K differ only by 15% in magnitude. Also, the transition temperature seems to be far above 700 K, as seen in Fig. 2.4a. The collected magnetic results indicate that, most likely, clusters with ferromagnetic interactions with a T_c well above 700 K are responsible for the observed magnetic behavior. Since no consistent explanation could be given and since there were strong doubts that the magnetic behavior was due to Mn substituting for Zn, the results have not been published. However, the results can serve as an example of how remarkable magnetization results need to be complemented with detailed structural studies before making (if possible) definite conclusions. Through magnetrometry at elevated temperatures (which is very seldom reported in papers making remarkable claims) one could almost immediately rule out intrinsic ferromagnetism in Mn:ZnO for the simple reason that such a well diluted magnetic system is incapable of delivering such a high T_c.

Co doped ZnO is probably the most studied oxide DMS [38]. In the Co:ZnO system, the ferromagnetic ordering was predicted to be from double exchange interactions between the Co ions [39]. Interestingly, high magnetic moments (2 μ_B/Co) and high magnetic transition temperatures [40] were initially reported, but generally the results for Co:ZnO have been very inconclusive (as is the case for Mn:ZnO) even when comparing results obtained for seemingly identical materials prepared using the same method. Several attempts have been made to explain the origin of the observed magnetic behavior, see e.g. Refs. [41, 42, 43, 36]. However, the consensus today is that the magnetic properties of TM-doped ZnO strongly depend on defects and on the chemical configuration of the dopant's.

2.1.1.1 Results: Co:ZnO

Since charge carriers have been suggested to mediate the FM interaction in TM:ZnO, we performed a study on $(Zn,Co_x,Al_y)O$ with $x = 5\%$ and $y = 0/0.8$ %, paper IV. The idea was to increase the number of electrons in the already highly *n*-doped ZnO using Al-doping. The structural characterization, XRD and scanning electron microscopy (SEM), indicated polycrystalline phase pure samples. The indications of phase pure samples were confirmed with no sign of metallic Co or other precipitates by measuring the electronic structure using synchrotron spectroscopy. Also seen, Co^{2+} resided on substitutional Zn sites, and the Al doping only affected (Zn,Co)O and not pure ZnO. These results are in good agreement with LSDA+U electronic structure calculations found in paper IV. DC magnetic measurements showed a paramagnetic behavior with no sign of spin ordering. The onset of magnetic saturation, seen in the inset of Fig. 2.5a, is expected since the Zeeman and thermal energies are of comparable magnitude for the high fields (∼30 kOe) and low temperature (T = 2 K) used in the experiments. Effective magnetic moments (μ_{eff}) have been extracted using the relationship $\mu_{\text{eff}} = \sqrt{\chi \cdot 3k_BT/\mu_0 N_T}$,

where $\chi = \partial M/\partial H$ from the low field slope of the M vs. H curve, N_T corresponds to the number of Co moments per unit volume, and is obtained from $N_T = 2x/V_{\text{cell}}$ where x is the relative Co concentration and V_{cell} is the wurtzite cell volume. Additionally, Co magnetic moments $\mu_{\text{HF}}(= M_s/N_T)$ were extracted from the M_s values measured at $H = 30\,\text{kOe}$ and the generated results are shown in Table 2.1.

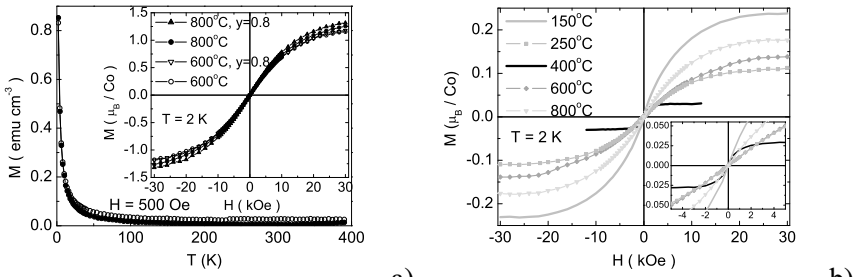

Figure 2.5: Magnetization (M) versus temperature (T) and field (H) measurements **a)** on $Co_{5\%}Al_{y\%}$:ZnO-samples annealed for 1 h in air at 600°C (open symbols) and 800°C (filled symbols) as well as with (triangles) and without (circles) y=0.8% Al. **b)** M versus H at $T = 2$ K for $Co_{15\%}$:ZnO samples annealed for 15 min in Ar at 150, 250, 400, 600 and 800°C (orange, orange squares, black, red diamonds and yellow triangles, respectively).

The expected magnetic moment for localized Co in an ionic 2+ state is 3 μ_{B}; the values for μ_{eff} are only slightly smaller while μ_{HF} is considerably smaller. The most likely cause of this behavior is antiferromagnetically coupled Co-rich clusters with uncompensated spins. The behavior can not be explained by non-interacting atomic magnetic moments or by ferromagnetically coupled Co moments. For antiferromagnetic nanoparticles with uncompensated spins, a model proposed by Néel [44] can be used to estimate the average number of atomic magnetic moments (n_c) in a cluster. The uncompensated magnetic moment in a cluster is proportional to n_c^q, where q= 1/3 and 1/2 for moments randomly distributed at the surface or in the volume, respectively. From the low field magnetization $\chi = N_T/n_c^{1-2q} \cdot \mu_0 m^2/3k_B T$, where m is the atomic Co magnetic moment (here put to 3 μ_{B}), a rough mean value for the number of Co spins present in each cluster can be estimated. Using the experimental values for μ_{eff} and $q = 1/3$, $n_c \approx 3$ is calculated. To estimate n_c for the high field region, the relationship $\mu_{\text{HF}} = 1/n_c^{1-q} \cdot m$ can be used and yields values for n_c between 4 and 6. The importance of this result is not the exact value of n_c but rather that the obtained values for μ_{eff} and μ_{HF} give a strong indication of the existence of small Co-rich clusters containing uncompensated spins. The small amount of Co spins present in each cluster will be very difficult to detect with structural measurements. Additionally, if the clusters are co-

herently incorporated in the structure they will be almost invisible even with standard high resolution imaging techniques [45].

Table 2.1: *Magnetic moments from the high field region (μ_{HF}) and effective magnetic moments (μ_{eff}) derived from the low field slope of the M vs. H curves for $Co_{5\%}$,$Al_{y\%}$:ZnO and different annealing temperatures.*

Annealing temp.	y	μ_{HF} (μ_B/Co)	μ_{eff} (μ_B/Co)	μ_{HF}/μ_{eff}
600°C	0	1.15	2.69	0.43
600°C	0.8	1.18	2.70	0.44
800°C	0	1.25	2.75	0.45
800°C	0.8	1.31	2.84	0.46

Magnetic and chemical pair interactions, calculated within the coherent-potential approximation (CPA), are presented in Fig. 2.6. The interactions are plotted as a function of Co-Co separation for different Co concentrations with and without Al co-doping. As seen in Fig. 2.6a, the magnetic interactions (J_{0j}) in Co:ZnO are ferromagnetic for low Co concentrations and decrease with increasing Co content to finally become antiferromagnetic for very high Co concentrations. Negative chemical pair interactions (V_{0j}) indicate a tendency for Co atom clustering. For both J_{0j} and V_{0j}, introduction of Al increases the interaction strength. From the calculations, one concludes that the observed magnetism in the system could be attributed to low concentration of randomly distributed Co atoms with interactions that are very localized in space. The tendency for Co clustering, enhanced by Al co-doping, generates regions of high Co concentration with AF interactions between the Co atoms. It is important to note that although the first neighbor interaction is very strong, the resulting T_c is quite low. This is because the probability of having nearest-neighbor spins is very low and hence the contribution to the total magnetic interaction is negligible for a low concentration spin system with homogeneously distributed spins.

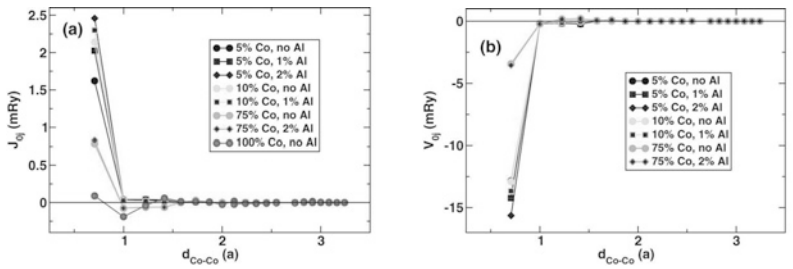

Figure 2.6: Calculated magnetic **a)** and chemical **b)** pair-interactions versus Co-Co separation distance for different Co concentrations in the presence and absence of Al_{Zn}.

To further investigate whether the magnetic behavior in Co:ZnO arises from AF Co-clusters, samples at the solubility limit were produced, described in paper III. The samples were fabricated through solution based alkoxide chemistry and subsequently heat treated in Ar atmosphere for 15 minutes at 150, 250, 400, 600 and 800°C. As seen in Fig. 2.5b, with the exception of the 400°C sample, the observed magnetic behavior closely resembles that observed for the $Co_{5\%}Al_{0/0.8\%}$:ZnO samples albeit with smaller magnetic moments. XRD studies (not shown) indicate phase purity in the 150, 250 and 400°C samples, while the XRD results for the 600°sample, show traces of spinels (Co_3O_4). Moreover, a weak CoO diffraction peak is observed for the 800°C sample. It should be noted that at and above 800°C the spinel phase decomposes to oxygen and CoO [46]. The Co_3O_4 spinel contains both octrahedral Co^{3+} and tetrahedrally coordinated Co^{2+} similar in the case of Co^{2+} substituting for Zn in ZnO. Spectroscopy measurements suggest that the 400°C sample is very similar to the 600°C sample, and evidence of $ZnCo_20_4$, which also seems more stable in these particular samples, is found. In contradiction with the XRD results, the spectroscopy measurements clearly indicate that secondary phases are present in all $Co_{15\%}$:ZnO samples which yields both di- and trivalent Co. Assuming that the magnetic behavior originates from antiferromagnetically coupled Co-rich clusters with uncompensated spins (used for the $Co_{5\%}$,$Al_{y\%}$:ZnO samples) along with the constraint that μ_{HF} and μ_{eff} should yield the same n_c, estimates of m and n_c can be calculated. The calculated n_c, given in Table 2.2, are independent of q, that is if the uncompensated spins are on the surface or in the volume of the cluster. The value for n_c stays fairly constant throughout the annealing series suggesting that the clusters are formed during synthesis and are only affected chemically during the heat treatment. Subsequent estimates of m are now possible. Samples annealed at intermediate temperatures show a decrease in magnetic moment to around 2 μ_B , most likely due to formation of Co^{3+} which is usually in its low spin state ($S = 0$) with 0 μ_B. The magnetic behavior of the 400°C sample differs from the behavior of the other samples in the series and could be explained by the Co^{3+} rich compound obtaining a weak ferromagnetic component under these conditions. Quesada *et al.* have shown that the pure Co spinel (Co_3O_4), which normally is in an AF state, can exhibit a weak FM behavior when mixed with ZnO [47]. Even for relative spinel concentrations as small as 1% (not visible in XRD), a hysteresis loop was detected at RT. The $ZnCo_20_4$ spinel has exhibited a FM and AF behavior when either p- or n-doped, respectively [48]. The observed M_s value for FM $ZnCo_20_4$ is on the same order of magnitude as that observed for the 400°C sample. Clearly, the results support the idea that the magnetic behavior in Co doped ZnO originates from the formation of small Co-rich clusters. Slightly surprising in these findings is that the cluster size seems to be fairly stable even for annealing temperatures as high as 800°C. The change in magnetic behavior with annealing temperature stems from the change in chemical composition.

Table 2.2: *High field magnetic moment (μ_{HF}), taken from the saturation magnetization, effective magnetic moment (μ_{eff}), calculated from the low field susceptibility, average magnetic moment (m) and cluster size (n_c).*

Annealing temp.	μ_{HF} (μ_B/Co)	μ_{eff} (μ_B/Co)	m (μ_B/Co)	n_c
150°C	0.24	1.66	3.16	48
250°C	0.12	0.97	1.95	65
400°C	0.031	1.40	-	-
600°C	0.14	0.98	1.87	49
800°C	0.18	1.27	2.44	50

Ion implantation is a widely used method to dope semiconductor crystals, and could in principle give a material of single crystal quality with uniformly distributed Co ions sitting in Zn sites. To recover the radiation damaged ZnO lattice, post implantation annealing is required which consequently enhances the risk of forming secondary phases. We have implanted commercially available ZnO single crystals with Co-ions at 100 keV and a fluence of 4.8×10^{16} cm^{-2}; results presented in paper II. The resulting nominal Co concentration was 10%. The samples were subsequently annealed at 500°C and 800°C for 1 h in Ar-gas.

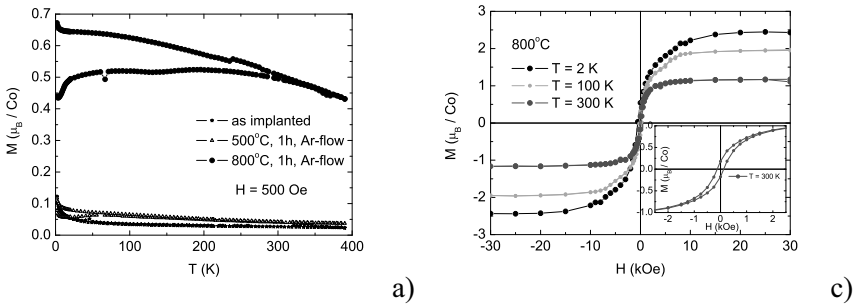

Figure 2.7: Magnetization measurements for Co implanted ZnO single crystals. As-implanted sample (stars), and samples annealed at 500°C (triangles) and 800°C (circles). **a)** ZFC and FC magnetization versus temperature. **b)** Magnetization versus field for the 800°C sample at 2, 100 and 300 K with the inset showing a zoomed in view of the 300 K measurement.

The as-implanted sample displays similarities to the previous results shown for Co:ZnO. The *M vs*. *T*-curve displays a paramagnetic behavior and in the *M vs*. *H*-curve a $M_s = 1.2$ μ_B/Co is seen. XRD results indicate a nearly phase pure sample with only a weak additional diffraction peak, identified as an hcp diffraction peak tentatively attributed to strongly strained hcp Co nanocrystallites. For the 500° sample, XRD shows a more pronounced hcp Co

peak as well as a diffraction peak possibly from Co_2Zn. As seen in Fig. 2.7a, a divergence between the ZFC and FC magnetization curves occurs below 100 K with a T_{cusp}^{ZFC} appearing at 70 K indicating blocking of nano-crystallite magnetic moments. Moreover, for the 500°C sample, M_s decreases to about 0.8 μ_B/Co. In addition, a coercive field (H_c) of 500 Oe is observed at 2 K. A similar hysteretic behavior is observed for the 800°C sample, seen in Fig. 2.7c, and in this case the behavior prevails above room temperature. The M_s=2.4 μ_B/Co at 2 K is somewhat lower than the spin only value for Co^{2+} and at 300 K a M_s=1.2 μ_B/Co is seen. The ZFC/FC magnetizations curves for the 800°C sample are larger in magnitude compared to that of the as-implanted and 500°C samples, and a divergence occurs between the curves at 310 K. The plateau, seen in the ZFC magnetization curve, extending from room temperature down to cryogenic temperatures could be interpreted as a distribution of crystallite sizes which yields a distribution of energy barriers for thermal activation and therefore corresponds to a broad distribution of blocking temperatures. The 800°C sample also displays an XRD peak attributed to fcc Co. None of the samples showed any sign of Co_3O_4 or $ZnCo_20_4$ spinels in the XRD measurements. Results from XPS measurements on both the 500°C and 800°C samples indicate that most of the Co sits on substitutional Zn sites. For the 500°C sample indications of Co^{2+} substituting Zn is found. In addition, the 800°C sample shows traces of Co^{+3} possibly originating from spinels as well as a contribution from metallic Co. The as-implanted ZnO sample exhibits weak magnetic interactions between the Co atoms. Upon heating, the Co starts to diffuse forming regions of high Co concentration. These regions create metallic fcc Co and possibly spinel nano-crystallites. The tendency to form regions rich in Co has previously been discussed in Ref. [49]. We have also shown, in paper IV, that for low concentrations of Co, short-range FM interactions are preferred but with increasing concentration the interactions become AF. The lower moment in the 500°C sample could be explained by a small amount of Co nano-crystallites providing an AF contribution, while not yet being metallic and FM. In the 800°C sample, the presence of metallic fcc Co is well established.

The claim that non-magnetic semiconductors should become ferromagnetic even at temperatures exceeding room temperature by doping with only a few percent of *TM*-ions is probably the most surprising claim, regarding magnetism, made this far in the 21th century [42]. The results above clearly show that this claim still needs proof. We have shown that the magnetic response for all DMS materials investigated in this thesis originates from secondary phases and/or precipitates; we stress that very small amounts of a secondary phase can dominate the magnetic behavior of a particular DMS film, even though the total measured magnetic moment in many cases is dominated by the substrate diamagnetic contribution. The Co-clusters do not necessarily need to be built up of randomly located Co atoms sitting in the lattice but rather nano-sized regions with high concentration of Co atoms occupying Zn-sites in the wurtzite

structure. A change in chemical composition of such regions will yield a new magnetic response. Sufficiently large clusters can result in magnetic hysteresis and a finite remanent magnetic moment even at room temperature- and can easily be misinterpreted as a ferromagnetic state of the DMS material. Since electronic devices can not contain even very small clusters of magnetic ions [50], oxide DMS devices will probably not see the light of day.

2.2 Metal Spin Injectors

Ferromagnetic metals are seen as strong candidates for spin injectors in semiconductor spintronics. The problem with spin flip scattering due to conductivity mismatch [51] can be surmounted by using tunnel contacts [52]. Manganese arsenide (MnAs) is very attractive for future spintronic applications because epitaxial films can be grown on ordinary semiconductors such as Si [53] and GaAs [54], and its T_c is above room temperature. Thus, MnAs is a good candidate for room temperature spin injectors in ferromagnetic-semiconductor heterostructures [55].

2.2.1 MnAs

The ferromagnetic properties of MnAs have been studied for more than 100 years [56]. The magnetic transition temperature of bulk MnAs was first reported in 1911 by Hilpert and Dieckmann [57]. At equilibrium in room temperature, bulk MnAs is ferromagnetic with a NiAs-type hexagonal structure (α-phase) with a_{hex}=3.71 Å and c_{hex}=5.71 Å. At T_c= 313 K a first order phase transition to an orthorhombic paramagnetic phase (β-phase) occurs with a_{ortho}=5.72 Å, b_{ortho}=3.68 Å, and c_{ortho}=6.38 Å. At an even higher temperature, 399 K, a second order phase transition appears where MnAs transforms back to the NiAs-type hexagonal structure (γ-phase) and still has paramagnetic properties. The first order magnetostructural transition shows a density increase of $\sim$1.9% [58], a latent heat of 7490 J/kg [59] and a 10° hysteresis in T_c [60] depending on whether you go up or down in temperature. At low temperature, M_s= 3.45 μ_B/Mn [61]. The magnetic anisotropy is comparatively strong in MnAs with the hard axis of magnetization along MnAs[0001] the hexagonal c-axis and the easy axis along MnAs[11$\bar{2}$0] hexagonal a-axis. Historically, the interest in MnAs is due to the first-order magnetostructural transition [62] and the magnetic state of the β-phase. Some reports have suggested that the β-phase is antiferromagnetic [63, 64], but this assertion was later disproved both experimentally [65] and theoretically [66, 67]. Despite the early conclusion, the controversy whether the β-phase is antiferromagnetic [68, 69] or paramagentic [67] is not yet settled. It has even been suggested that if the structural α/β-phase transition did not occur the T_c of MnAs would increase to 399 K, the γ-phase transition [63, 67]. Effects induced by altering the volume and/or lattice parameter by means of pressure [70, 71] and magnetic field [72] have also been of great interest. By applying a presssure, a two-phase region (α/β) can be induced below T_c; and for sufficiently high applied pressures ($>$ 4.3 kbar) the β-phase will prevail to very low temperatures. Even when the pressure is removed the α-phase cannot be restored until the material is heated above 160 K [60]. MnAs has also been found to exhibit a large magnetocaloric effect, both in bulk form [73, 74] and as a thin film [75].

MnAs films are mostly grown on GaAs substrates with a low temperature (200 - 240°C) molecular beam epitaxy (MBE) growth and display excellent heteroepitaxy [54]. By choosing substrate and growth conditions, the direction of MnAs[0001] with respect to the substrate can be altered. For instance, when put on a GaAs(111) substrate, the MnAs[0001] points out-of-plane relative to the substrate plane while the GaAs(100) substrate yields an in-plane orientation of MnAs[0001].

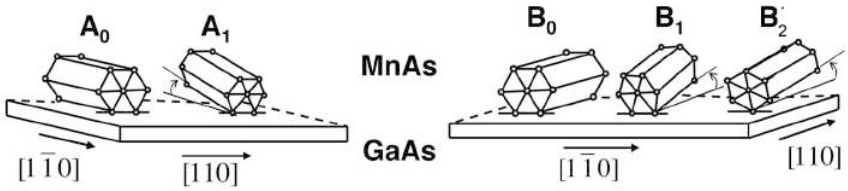

Figure 2.8: Crystal orientations of the hexagonal α-MnAs phase on GaAs(100). The MnAs[0001] crystal orientation types A_1, B_1 and B_2 are tilted with respect to the GaAs(100) substrate. After Iikawa *et al.* [76]

The substrate surface reconstruction controls the orientation as well as the azimuthal alignment of the MnAs film. To obtain the A_0-orientation preferable for applications (MnAs[0001]||GaAs[1$\bar{1}$0] shown in Fig. 2.8), a very As rich reconstruction ($d(4\times4)$) is required to create an almost amorphous surface. A less As-rich surface reconstruction ($c(4\times4)$) results in a B-type orientation. An A_1 (or B_1) orientation with an angle (α) between c_{hex} and the substrate surface is obtained with Mn-rich growth conditions [76]. One complication we have observed regarding the very thinnest films (<70 Å) is at the beginning of the film growth MnAs nucleates as islands. Consequently, a comparably rough surface is created for the thinnest films.

2.2.1.1 Results: MnAs/GaAs

MnAs films with a nominal thickness of 1000 Å were grown on GaAs(100) substrates with either a $d(4\times4)$ or $c(4\times4)$ surface reconstruction, presented in paper I. To prevent surface oxidation, all samples were capped with a 1000 Å thick amorphous As layer directly after film growth. The de-cap sample was heat treated (at 310°C for 60 minutes) prior to synchrotron measurements in order to remove the As capping layer. Despite the relatively low temperature and short annealing time used during de-capping, a clear difference is seen between the As-cap and de-cap samples where M_s= 3.92 and 3.79 μ_B/Mn at 10 K, respectively. XRD results reveal that the heat treatment has relaxed the structure resulting in a higher concentration of the A_0 orientation (from 86 to 95 %). The presence of additional orientations to A_0 in the film explain the deviation from a perfectly rectangular shape of the magnetization versus field curve, shown in Fig. 2.9b. The small amount of B-orientation present both in the As-cap and de-cap sample, gives a hard axis contribution to the

measured magnetization curve and is clearly visible at low applied fields. The ratio M_s/M_r, where M_r is the remanent magnetization, was used to estimate the fraction of B-orientation in the film, and the results compare favorably with the fractions obtained from XRD. The $c(4\times4)$ sample exhibits a lower $M_s = 3.23\ \mu_B$/Mn but the highest T_c= 335 K. By comparing the three samples we see that as c_{hex} increases T_c decreases, which opposes results from earlier investigations on MnAs/GaAs(100) films using *three-point-bend* measurements; these investigations concluded that T_c should increase with stretching of the c_{hex}-axis [77]. B_1 (72%) is the main orientation in the $c(4\times4)$ film, which could explain the larger T_c since it has been argued that the transition temperature will increase as MnAs[0001] obtains an out-of-plane orientation [76]. This is also the proposed explanation for why MnAs/GaAs(111) films most often display the highest T_c values. The magnetocrystalline anisotropy (MCA) has a 90° relationship between the easy axis, MnAs[11$\bar{2}$0], and the hard axis, MnAs[0001], of magnetization. In the expression for the free energy density (F), given by Eq. (1.4), the fraction of each c_{hex} out-of-plane orientation (a_0, $a_1\ldots$) has to be considered as well as their respective angle (α_0, $\alpha_1\ldots$) with respect to the substrate, yielding:

$$\begin{aligned} F &= K_1[a_0\cos^2\alpha_0 + a_1\cos^2\alpha_1 + \ldots]\sin^2\theta + \\ &\quad + K_2[a_0\cos^2\alpha_0 + a_1\cos^2\alpha_1 + \ldots]\sin^4\theta - \\ &\quad - \mu_o H M_s\cos\theta. \end{aligned} \tag{2.1}$$

The derived values of K_1 and K_2 (see Table 2.3) show that MnAs/GaAs has a so-called *easy*-plane anisotropy. The derived K-values for the $d(4\times4)$ and GaAs(111)B samples at low temperature are larger than what has been found in bulk MnAs [62], but the K-values are smaller than the bulk values above 280 K. This is most likely due to the two-phase region that is present in MnAs thin films (but not in bulk) since the MCA depends on the spin-orbit coupling. The results also indicate that the α/β coexistence region extends to lower temperature ($<$283 K) than previously reported [78]. The change in behavior is also reflected in the results obtained from XMCD measurements, where the orbital moment (m_l) decreases more slowly with increasing temperature than the spin moment (m_s). The observed difference in the temperature dependence of m_s and m_l is well in accord with expectations for a structural phase transition. From temperature dependent transmission electron microscopy (TEM) diffraction studies an increase of the c/a-ratio for $T>250$ K is seen. The results for K_1, K_2 and m_l/m_s suggest an onset of the β-phase somewhere in the temperature range $250<T<280$ K as well as a change in magnetic moment and anisotropy with lattice strain.

In our investigations of MnAs we have had support from the theoretical magnetism group at Uppsala University who performed *ab initio* density functional theory (DFT) and dynamical mean field theory (DMFT) calculations. The calculated magnetic moment, 3.13 μ_B/f.u., is lower than seen in our ex-

Table 2.3: Anisotropy constants K_1 and K_2 measured at different temperatures (T_m), T_c, room temperature c-axis length and c/a-ratio and fraction of each in- or out-of-plane orientation for the different samples of 1000 Å thick films on GaAs(100) (As-cap, de-cap and $c(4\times4)$). The corresponding results for a 1000 Å thick film deposited on GaAs(111)B are also given. Bulk values from Ref. [62] are included for comparison.

sample	T_m (K)	$K_1(\times10^5$ J/m$^3)$	$K_2(\times10^5$ J/m$^3)$	T_c (K)	c_{hex} (Å)	c/a
As-cap	10	-14.0	1.4	317		
	100	-13.9	1.3			
	200	-12.4	1.2			
	250	-10.3	0.9			
	280	-8.4	0.9			
	290	-7.5	0.9			
	300	-6.2	0.6		5.772	1.555
	305	-5.9	0.4			
de-cap	10	-14.4	1.7	320		
	100	-14.4	1.7			
	200	-12.8	1.5			
	250	-10.6	1.2			
	280	-8.8	1.1			
	290	-7.9	1.1			
	300	-6.5	0.8		5.755	1.551
	305	-5.8	0.6			
c(4×4)	10	-7.3	1.5	335		
	100	-5.6	1.1			
	200	-4.8	0.9			
	300	-3.2	0.8		5.746	1.544
	320	-2.9	0.9			
GaAs(111)B	10	-13.9	1.1	335	-	-
	100	-14.0	1.2			
	200	-12.4	1.1			
	300	-4.5	0.3			
Bulk	77	-12.0	-	313		
	198	-11.0	-			
	273	-9.0	-			
	299	-7.6	-		5.712	1.540

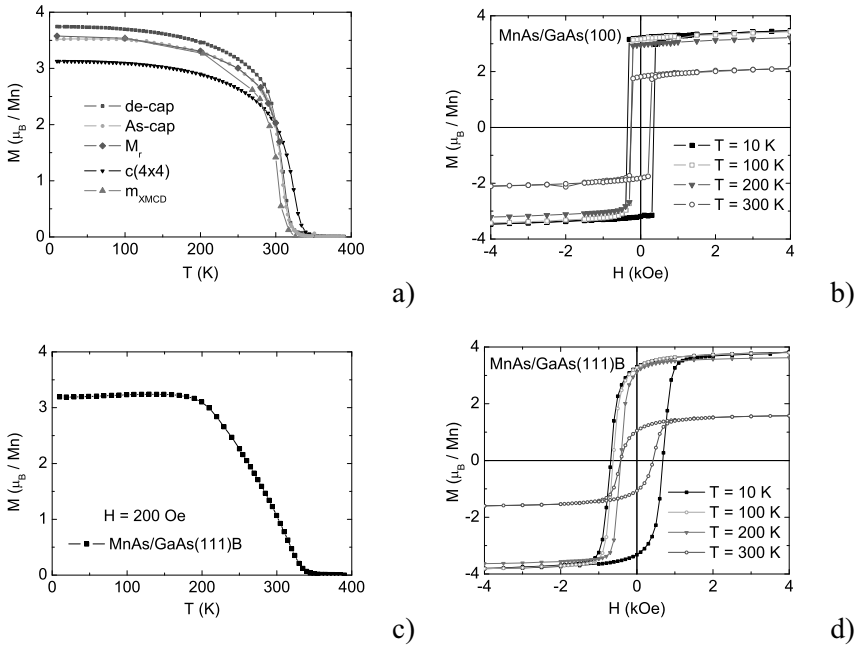

Figure 2.9: **a)** Results for MnAs/GaAs(100) films. Magnetization versus temperature for the de-cap, As-cap and c(4 x 4) samples. The remanent magnetization (M_r) for the de-cap sample and the XMCD magnetic moment (m_{XMCD}) are included for comparison. The XMCD data have been normalized with respect to the remanent magnetization at 100 K. **b)** Magnetization versus field for the As-cap sample. **c)** Magnetization versus temperature for MnAs/GaAs(111)B. **d)** Magnetization versus field for MnAs/GaAs(111)B.

periments while the value for the MAE, 0.25 meV/f.u. ($\approx 12\times10^5$ J/m^3), is in good agreement with the experimental values. The theoretical results show that the magnetic properties depend strongly on lattice strain, especially on variations of a_{hex}. Even a small relaxation of the structure seemingly affects the magnetic properties. This is the case for the de-cap sample for which we observe an increase in the fraction of A_o orientation together with a slight T_c increase and decrease in M_s. Considering that theoretical calculations tend to underestimate the magnetic moment for MnAs (3.06 μ_B/Mn) [79, 80], our experimentally measured values are fully plausible. It should be noted though that large theoretical $M_s(\sim 4\ \mu_B)$ values as a result of lattice distortion [81] have been reported. Even though the distortion requires unphysical a_{hex} and c_{hex} values, the important observation is the large change in magnetic moment with lattice distortion.

The experimentally observed large magnetic moments and MCA arise from locally strained regions in the samples. Also, our results indicate that the two-phase region starts at a temperature close to 250 K. This is evident from the

magnetization versus field results where after having subtracted the diamagnetic background of the substrate, even at 250 K an additional paramagnetic component from the β-phase is clearly resolved beside the FM signal from the α-phase.

The MnAs/GaAs(111)B[6] films generally exhibit higher T_c compared to the MnAs/GaAs(100) films. Our results show that T_c increases in MnAs/GaAs(111)B films with decreasing film thickness. These observations further support the notion that the magnetic properties are more dependent on a_{hex} strain than on c_{hex} strain. In the MnAs/GaAs(111)B one must also consider the shape anisotropy ($K_{sh} = -1/2 \cdot \mu_0 M_s^2$) when extracting values for K_1. The more rounded shape of the *M vs*. *H*-curves, seen in Fig. 2.9c-d, are due to a vortex like domain pattern [54] created by the existence of three azimuthal orientations of the magnetic domains. The probable cause of the higher moments in MnAs films compared to bulk MnAs is strain of the in-plane axes with large distortions locally. Strangely enough, other groups have published lower M_s values or only shown plots of M/M_s. The *MCA* is stronger in thin film than in bulk MnAs, and also shows a comparably strong dependence on a_{hex} strain.

[6]Since GaAs is polar in the (111) plane either Ga or As can be the element closest to the surface, in the case of 'B' it denotes that As is the top most element.

3. Frustrated oxides

Spin glasses are totally useless piece of materials, however constitute convenient laboratory frame for theoretical and experimental investigation. [1]

The motivation for performing research on magnetically frustrated systems is in most cases not the ability to create a material for future practical applications but rather that random and frustrated spin systems conceivably will give us a more fundamental understanding of disordered matter. Frustrated spin states, such as those found in spin glasses, appear most often at temperatures far below the low temperature limit for device systems. Despite this setback, spin glass behavior has spurred a lot of research interest. The knowledge gained in spin glass research has proved to be of use in various spin-off areas such as neural networks, computer optimization, heteropolymers [83, 84] to list a few. Additionally, more direct applications can be envisioned since a frustrated behavior gives information about structural disorder or mixed valence states of transition metal ions affecting the transport properties at elevated temperatures. This is a perfect example of how the low temperature magnetic behavior yields information directly linking to the the electrochemical properties of materials used in batteries, as discussed in section 3.2.1.

Words such as disorder, frustration and spin glass are sometimes used interchangeably to describe properties of a magnetic material. However, some differences in the meaning of these words can be distinguished. A good example of a spin glass is CuMn in which the Mn-ions are randomly dispersed in the Cu matrix. The Mn content is typically somewhere in the range of 5 - 10 atomic percent and the interactions between Mn-ions are of RKKY-type (i.e. the interactions will vary between AF and FM with respect to the distance between the Mn-ions). This results in a frustrated spin state with FM and AF interactions. A different example is the site-ordered but frustrated state (geometrical frustration) in which all interactions are of AF type but still cannot be simultanously satisfied, as seen in Fig. 3.1c. A commonly used parameter is the frustration factor $f_f = |\theta_w| / \mathrm{T}_f$, where T_f represents any cooperative-ordering transition temperature [85] such as T_g or T_c, and θ_w is the Weiss temperature. The requirement for a geometrically frustrated spin system is $f_f > 10$. Good examples of geometrically frustrated materials are the pyrochlorides which are built up of corner-sharing tetrahedras. The pyrochloride $Dy_2Ti_2O_7$, a spin ice compound, is thought to contain magnetic monopoles at very low temperatures ($\mathrm{T} < 2$ K) [86, 87, 88]. On the other hand, artificial spin ice systems con-

[1] J. P. Bouchaud in [82]

sisting of regular arrays of magnetic thin film elements forming honeycomb or squares lattices, are believed to have magnetic monopoles at room temperature [89, 90]. This phenomenon could greatly impact in the area of magnetic data storage [91]. It's evident that the time has come to revise Bouchaud's statement and to realise the importance and potential in understanding fundamental properties even at cryogenic temperatures.

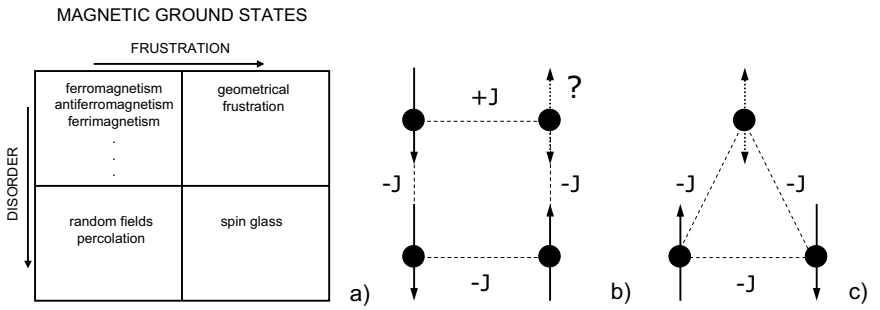

Figure 3.1: **a)** Ground states of magnets from the perspective of site disorder and frustration. Illustration of the difference between **b)** the structurally disordered and **c)** the geometrically frustrated spin systems and resulting magnetic states. After Ramirez [85].

A lattice containing some sort of triangular structure, and to some degree AF interactions will inevitably demonstrate magnetic frustration. Both materials presented below show a triangular type structure containing AF interactions and a mixed valence state - the perfect prerequisites for magnetic frustration.

3.1 Perovskite: La-doped SrMnWO

Research on perovskite [2] materials has resulted in important physical discoveries such as the double-exchange interaction as well as the Jahn-Teller polaron [92]. The family includes high-T_c superconductors [93] and half-metallic ferromagnets with a T_c at room temperature displaying colossal magnetoresistance [94]. Perovskite materials consist of two cations and three oxygen anions with a general formula of $AB'O_3$ where A stands for an alkali or rare earth metal and B' for a transition metal. These materials are build up of corner sharing octahedras ($B'O_6$) with A occupying every hole created by the eight $B'O_6$ octahedras. The structure is often distorted to a lower symmetry (tetragonal, orthorhombic etc) than that of the ideal cubic structure. The double perovskite general formula is $A_2B'B''O_6$ with four $B'O_6$ and $B''O_6$ octahe-

[2] named after the Russian discoverer of the equistructural $CaTiO_3$ mineral

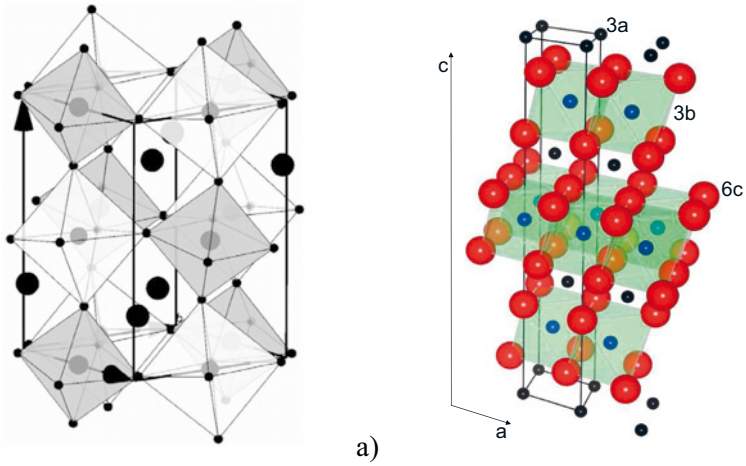

Figure 3.2: **a)** Monoclinic double perovskite $Sr_{1.5}La_{0.5}MnWO_6$. Sr/La atoms are shown as large black spheres; oxygen atoms are shown as small black spheres at the corner of octahedra. Mn and W are located inside the white and gray octahedra, respectively. **b)** Hexagonal α-$NaFeO_2$-type structure (space group $R3m$) with lithium (black balls) at the 3a-site, TM's (blue balls) at the 3b-site and oxygen (red balls) at the 6c-site.

dras ordering in a chess board type fashion around the A metal, as shown in Fig. 3.2a. Most of the phenomena discovered in perovskites are due to carrier doping which induces a mixed valence state of the transition metal (usually Mn). In our case, electron doping is achieved by substitution of the divalent strontium (Sr) with trivalent lanthanum (La), as noted in paper IX.

3.1.1 Results: SrLaMnWO

Samples of $Sr_{2-x}La_xMnWO_6$ with x = 0, 0.25 and 0.50 were prepared using solid state methods. The undoped form (x = 0) displays a tetragonal structure (space group $P4_2/n$). In the La-doped samples (x = 0.25 and 0.50) the structures change to a monoclinic structure (space group $P2_1/n$) shown in Fig. 3.2a. The structural parameters were obtained from Rietveld refinement using the FULLPROF method [95] of neutron powder diffraction (NPD) data. Upon electron doping, tungsten (W) exhibits a mixture of +6 and +5 oxidation states, while the Mn^{2+} is stable [96]. As evidenced from earlier investigations in the group [97], the parent compound shows a short-range canted AF state at 50 K and a long-range AF state develops below T_N=13 K. A Weiss temperature (θ_w) of -78.5 K is derived from a high temperature Curie-Weiss (CW) fit, $\chi = C/(T - \theta_w)$, also see Table 3.1. In the La-doped samples, no long-range AF order is detected in the magnetization data, but NPD results show that short-range correlated AF regions are present at 5 K in the x= 0.25 sample. For both, x= 0.25 and 0.5, samples, the ZFC/FC suscepti-

bility (χ_{ZFC}/χ_{FC}) results, shown in Fig. 3.3a and 3.3b, reveal both a field dependent divergence between the ZFC and FC curves and a field dependent cusp temperature (T_{cusp}). Both the magnitude of χ_{ZFC} and χ_{FC} and the temperature of divergence (T_r) between the ZFC/FC curves decrease with increasing applied magnetic fields. The T_{cusp}^{FC} increases with increasing field while T_{cusp}^{ZFC} approximately stays the same for the fields used here. These characteristics are clear indications of a low temperature spin glass state. The data from the high temperature *CW*-fit are given in Table 3.1. The decrease in $|\theta_w|$ with increasing electron doping indicates that the AF interactions are weakened due to electron doping. The change of sign in θ_w between the x= 0.25 and 0.50 samples indicates that the predominant interaction switches from AF to FM. It should be noted that the extracted μ_{eff} values are in good agreement with the spin only value for Mn^{2+} (S=5/2), 5.92 μ_B. From measurements of the

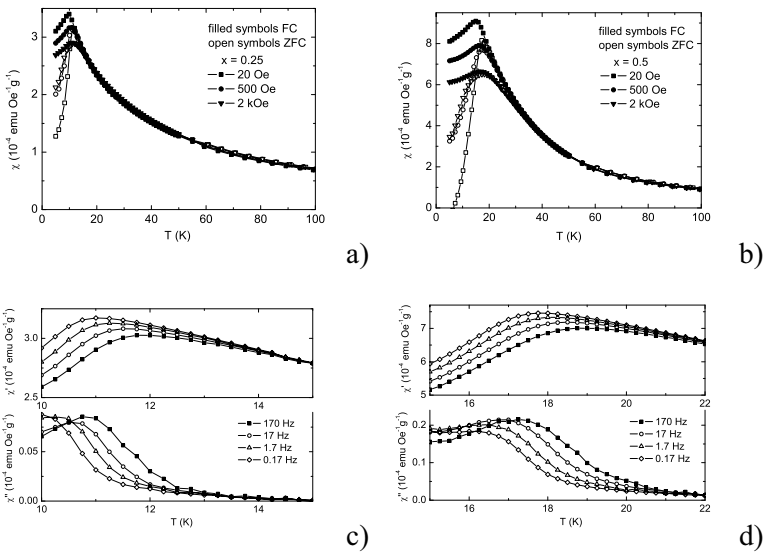

Figure 3.3: ZFC and FC susceptibility versus temperature for the **a)** x=0.25 and **b)** x=0.50 samples. The different curves correspond to different applied dc magnetic fields. **c)** and **d)** show AC susceptibility versus temperature for the x=0.25 and 0.50 samples, respectively. The different curves correspond to different frequencies of the AC magnetic field.

AC susceptibility versus temperature, shown in Fig. 3.3c and 3.3d, a clear frequency dependence is seen in both the in-phase ($\chi'(f)$) and out-of-phase ($\chi''(f)$) susceptibility further indicating a low temperature spin glass state. Assuming critical slowing down of the spin dynamics, dynamic scaling was performed according to Eq. (1.8) with T_f defined as the cusp temperature of χ'. The obtained values, shown in Table 3.1, for the critical exponent ($z\nu$) and the microscopic relaxation time (τ_o) are well in line what would be ex-

pected for a three dimensional (3D) spin glass [7]. The spin glass transition temperatures (T_g) corresponds well with the expectations from the DC susceptibility results. The spin glass behavior induced by electron doping is due

Table 3.1: *Data extracted for $Sr_{2-x}La_xMnWO_6$, x = 0, 0.25 and 0.50; lattice constants a and c, Weiss temperature (θ_w) and effective magnetic moment (μ_{eff}) derived from the high temperature Curie-Weiss fit, $\chi = C/(T-\theta)$, spin glass transition temperature (T_g), critical exponent ($z\nu$) and microscopic relaxation time (τ_o) derived from dynamic scaling analysis.*

x	a (Å)	c (Å)	θ_w (K)	μ_{eff} (μ_B/Mn)	T_g (K)	$z\nu$	$\tau_o \times 10^{-13}$ (s)
0	8.0119	8.0141	-78.5	6.10	-	-	-
0.25	5.6763	8.022	-4.8	5.57	9.9	13.2	2.9
0.50	5.6792	8.0256	24.5	5.35	16.5	11.0	4.3

to the formation of both AF and FM interactions. For x= 0, only W^{6+} exists with a filled $5d^0$ shell and there are no nearest-neighbor interactions between Mn^{2+} and W^{6+}, but an AF superexchange interaction of 180°-type between next-nearest-neighbors (Mn−O−W($5d^0$)−O−Mn) yields an AF state [5] at low temperature. The substitution of Sr^{2+} for La^{3+} creates W^{5+} ($5d^1$), which acts as a Pauli paramagnetic ion, whose exchange polarization supports FM Mn-Mn interactions [96]. Two Mn^{2+} ions experience an indirect exchange interaction (Mn−O−W($5d^1$)−O−Mn) where both Mn^{2+} ions interact antiferromagnetically with W^{5+} through the O $2p$ orbital. The resulting interaction between the two Mn^{2+} ions will therefore be FM. Since La^{3+} substitutes for Sr^{2+} at random positions, the FM interactions will be distributed randomly in the lattice, thus creating the prerequisite conditions for a low temperature spin glass state with a disordered mix of competing AF and FM interactions. The increase of T_g and the magnitude of the susceptibility with increasing electron doping can be explained by the increasing number of FM interactions which lead to a higher degree of spin frustration.

3.2 Li-layered oxides

From both theoretical and experimental point-of-views, layered transition metal oxides of α-$NaFeO_2$-type (space group $R\bar{3}m$) are highly interesting materials that were initialy predicted as being the first realization of a resonant valence bond (RVB) system[3] in $LiNiO_2$ [99, 100]. As seen in Fig. 3.2b, the α-$NaFeO_2$ structure consists of planes of alkali metals (e.g. Li or Na) alternating with metal oxide slabs (MO_2), where the edge-sharing

[3] also known as a (quantum) spin liquid. In the case of a quantum spin (S=1/2) system, if every pair of neighboring quantum spins forms an entangled spin singlet (valence bond), and if these singlets are quantum mechanically resonating among themselves [98] an RVB-state is formed.

octahedras (MO_6) form a two dimensional triangular lattice (2DTL). Due to similarities in the atomic radii between Li^+ (r_{Li^+}=0.72 Å) and Ni^{2+} ($r_{Ni^{2+}}$=0.69 Å), the parasitic Ni^{2+}_{3a} resides in the Li-layer (3*a*). Cationic mixing (Ni^{2+}_{3a}) creates interlayer interactions of both AF and FM type [101, 102] and as little as 1% Ni^{2+}_{3a} induces a spin glass state in $LiNiO_2$ [103]. Cationic mixing is in part the cause for the long term controversy of the magnetic ground state in $LiNiO_2$. To obtain a true 2DTL, the interlayer interactions must be minimized by reducing the cationic mixing as in $NaNiO_2$ [104] or by increasing the MO_2-plane distance as in Ag_2NiO_2 [105]. The true magnetic ground state of $LiNiO_2$ has recently been proposed to be of short-range AF 90°-type [106].

Interests in Li layered compounds have prompted a tremendous research effort due to their application in Li-ion batteries. The first demonstration of a reversible Li insertion was performed on Li_xTiS_2 in 1976 [107]. A few years later Li_xTiS_2 was outperformed by $LiCoO_2$ with respect to energy density [108] and battery cell size. Li-ion batteries, based on $LiCoO_2$, were commercially introduced in 1990 by Sony Corp. They are currently used in portable electronics, power supplies, medical instrumentation as well as in military, aerospace and automotive applications and are likely to be among the most important energy storage devices of the future [109]. Despite the excellent properties as a cathode, $LiCoO_2$ has some major drawbacks such as: high cost of Co, toxicity and instability at higher electric potentials. Presently, one seeks to partially of fully replace Co with other *TM*-ions while maintaining the structural stability and increasing the capacity. A possible candidate cathode material would be $LiNiO_2$ because of its low cost and high capacity, but stoichiometric order in $LiNiO_2$ is very hard to achieve. Another promising candidate is $LiNi_{1-y}Co_yO_2$, but the electric conductivity is low and hence the electrochemical properties will deteriorate upon cycling. When introducing Mn^{4+}, a mixed valence state of Ni (+2 and +3) is created enhancing the electrical conductivity. The compound $LiNi_{1/3}Co_{1/3}Mn_{1/3}O_2$ has been introduced as a commercial product, but no obvious reason has been presented as to why this particular composition has been chosen [110]. The presence of *TM*-ions will induce intra- as well as interlayer magnetic interactions. Thus, understanding the magnetic behavior will help to explain the electrochemical and structural properties of the compound.

Before analyzing the results for the battery compounds the possible magnetic superexchange interactions following the so-called Goodenough-Kanamori rules (see for instance refs. [111, 4, 5]) should be identified. First, in all the compounds, Co is assumed to be trivalent and in its low spin state (S= 0) and Mn in a tetravalent state even upon Li-extraction. Even though traces of divalent [110] and tetravalent [112] Co have been reported, the Co S= 0 approach is very common when analyzing the magnetic behavior in this material class and has also been adapted in this thesis. The present

TM-ions, Ni^{2+} ($e_g^2 t_{2g}^6$, S=1), Ni^{3+} ($e_g^1 t_{2g}^6$, S=1/2) and Mn^{4+} ($e_g^0 t_{2g}^3$, S=3/2), yield superexchange interactions as illustrated in Fig. 3.4.

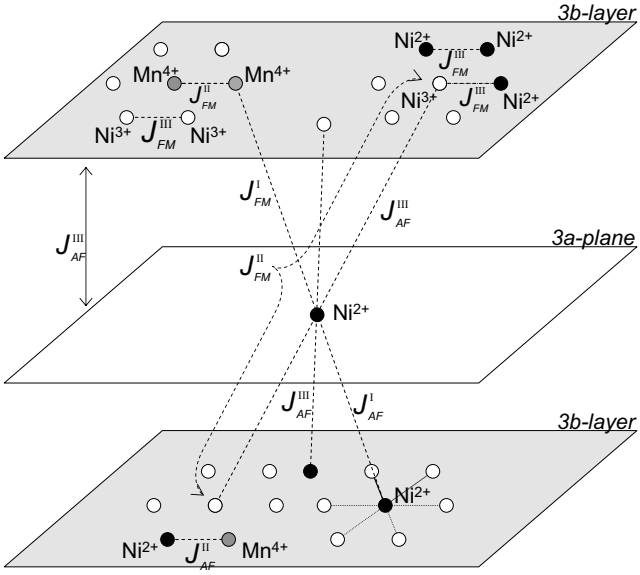

Figure 3.4: Schematic view of the interactions present in the Li(NiCoMn)O_2 samples, with the oxygen and lithium atoms omitted for clarity. The 180° interactions are illustrated between the planes and the 90° within the planes. The ferromagnetic, J_{FM}, and antiferromagnetic, J_{AF}, interactions with the roman superscript indicating the relative strength, $J_{AF}^{\mathrm{I}} > J_{AF}^{\mathrm{II}} > J_{AF}^{\mathrm{III}}$.

3.2.1 Results: Li(NiCoMn)O_2

Results from measurements on $LiNi_{0.65}Co_{0.25}Mn_{0.10}O_2$ samples with various heat treatments are presented in paper VIII. The samples were prepared by a combustion method and subsequent heat treatment in air at 900°C for 1 h (sample C_1), 900°C for 12 h (sample C_2) and at 1000°C for 12 h (sample C_3). The resulting samples had the desired rhombohedral α-$NaFeO_2$ structure, with lattice parameters listed in Table 3.2. The magnetic measurements shown in Fig. 3.5 show a Curie-Weiss behavior in the high temperature region for the C_1 and C_2 samples. The AF interactions dominate in the C_1 and C_2 samples while the C_3 sample shows a ferrimagnetic type behavior with a transition around 127 K seen in the inverse susceptibillity ($1/\chi$) measurement. The non-linearity of $1/\chi$ for the C_3 sample at high temperatures is due to a comparably large magnetization and is most likely caused by a small amount of impurity phase with a ferromagnetic transition temperature (T_c) well above 400 K. A

ferrimagnetic type behavior is also seen for C_1 and C_2 at lower temperatures.

Table 3.2: *Data for $LiNi_{0.65}Co_{0.25}Mn_{0.10}O_2$ heat treated at 900°C for 1 h (sample C_1), 900°C for 12 h (sample C_2) and at 1000°C for 12 h (sample C_3); a_{hex}, c_{hex} and cation mixing (z) extracted from Rietveld refinement [113] of powder XRD data, Weiss temperature (θ_w) and effective magnetic moment (μ_{eff}) derived from the high temperature Curie-Weiss fit, $\chi = C/(T-\theta)$ and ferrimagnetic transition temperature (T_c).*

sample	a_{hex} (Å)	c_{hex} (Å)	z (%)	θ_w (K)	μ_{eff} (μ_B/TM)	T_c (K)
C_1	2.8608	14.188	3	-87.5	2.22	-
C_2	2.8660	14.193	6	-39.1	2.13	85
C_3	2.8725	14.217	11	-	-	127

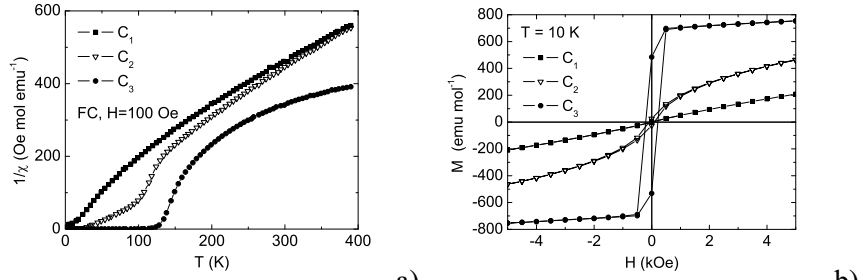

Figure 3.5: **a)** Inverse susceptibility ($1/\chi$) versus temperature and **b)** magnetization versus field of the C_1 (filled squares), C_2 (open triangles) and C_3 (filled circles) samples.

The results for C_1, C_2 and C_3, show the importance of Ni_{3a}^{2+} which couples to 6 neighboring ions (3 in each 3*b*-layer) [102] in the MO_2-slab and which induces AF and FM interactions of different strength. It should be mentioned that in AC susceptibility measurements (shown for C_2 and C_3 in Fig. 3.6) all samples exhibit a χ' and χ'' frequency dependent response but at different temperatures. The C_3 sample shows a frequency dependent AC susceptibility magnitude, but no frequency dependence of the cusp temperatures in χ' or χ'' (T_{cusp}=110 K) can be resolved. This kind of frequency dependence is what would be expected for a paramagnetic to a ferri- or ferromagnetic phase transition. Moreover, the magnetization versus field results (cf. Fig. 3.5b) show this sample to be a comparatively magnetically well ordered sample. Still, the AC susceptibility results reveal a weak anomalous behavior at lower temperatures ($\sim$ 65 K), a shoulder in χ' and a frequency dependent peak temperature in χ'', as seen in Fig. 3.6b. The C_2 sample displays a frequency dependence of

both the AC susceptibility magnitude and T_{cusp} and so resembles the behavior of a 3D spin glass. Assuming critical slowing down (according to Eq. (1.8)) dynamic scaling analysis yields a T_g= 19.7 K, $z\nu$= 6.8 and $\tau_o = 2.7\times10^{-11}$ s, clearly suggesting a 3D spin glass phase below 19.7 K. The C_1 sample shows a similar frequency dependent response with peak temperatures at ∼8 K. However, the magnetization of this sample is weaker than for the other two samples and the measured χ'' was approaching the resolution limit of the MPMS system; therefore no closer analysis of the spin dynamics was possible for this sample.

The smaller amount of cationic mixing in the C_1 sample together with smaller grain size (detected in SEM, see paper VIII) yield better cycling properties, lowers the Li diffusion distances and increases the surface area which make this sample more suitable as a cathode material in battery applications.

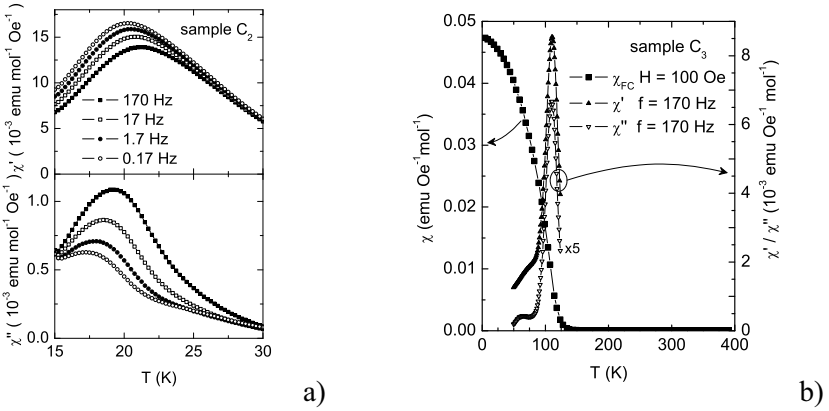

Figure 3.6: **a)** χ' (upper panel) and χ'' (lower panel) versus temperature for the C_2 sample. The different curves correspond to different frequencies of the AC magnetic field. **b)** χ_{FC} (filled squares), χ' (filled triangles) and χ'' (open triangles) versus temperature for the C_3 sample.

To gain insight about changes in structural and magnetic properties upon Li removal (charging of a battery) a new C_1 sample was fabricated and used as the cathode in a galvanic cell in order to withdraw Li through electrochemical charging. Five samples of $Li_xNi_{0.65}Co_{0.25}Mn_{0.10}O_2$ with x = 1, 0.9, 0.8, 0.65 and 0.5 (C_1^{x1}, C_1^{x09}, C_1^{x08}, C_1^{x065} and C_1^{x05}) were fabricated for the magnetic study. Through Rietveld refinement on powder XRD data, the cationic mixing for the C_1^{x1} sample was found to be 2.9%. During Li-extraction, for x=1→0.5, a small gradual decrease in a_{hex} (about 1.4%), due to Ni oxidation, as well as a c_{hex} expansion (about 1.5%), assisted by the increased electrostatic repulsion between the MO_2 layers, were observed. Only peaks attributed to redox reactions caused by Ni^{2+}/Ni^{3+} and Ni^{2+}/Ni^{4+} were observed in the electro-

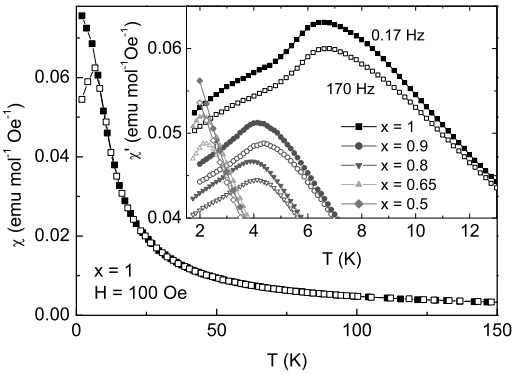

Figure 3.7: Results from magnetization measurements on $Li_xNi_{0.65}Co_{0.25}Mn_{0.10}O_2$; ZFC and FC susceptibility (open and closed symbols, respectively) versus temperature for x=1, with the inset showing χ' versus temperature for x=1, 0.9, 0.8, 0.65, 0.5 at f= 0.17 and 170 Hz (closed and open symbols, respectively).

chemical measurements. The Co^{3+} and Mn^{4+} ions remain inactive since their oxidations occur at higher potentials (>4.3 V). As seen in Fig. 3.7, the C_1^{x1} sample shows a clear divergence between the ZFC and FC susceptibily curves (at 6.6 K). The AC susceptibilty exhibits frequency dependent properties reminiscent of a spin glass material. Similar properties are observed for all samples, but the characteristic features (such as the onset of magnetic irreversibility) are pushed to lower and lower temperature with increasing Li-extraction and for C_1^{x05} this occurs even below the low temperature limit of the MPMS system. Upon removal of Li^+, Ni_{3b}^{2+} will oxidize to Ni^{3+} and subsequently to Ni^{4+}. Also, a small migration of Ni^{2+} to the 3*a*-plane will occur. This will remove some of the intra- as well as the interlayer AF couplings while the FM interactions (mostly $Ni_{3a}^{2+}-O-Mn_{3b}^{4+}$) will be remain unchanged or even increase. Upon oxidation, the exchange coupling distribution will become narrower thus lowering the spin glass temperature [114]. For x$\leq$0.65, the dominant interaction changes from AF to FM, which is a possible explaination for the larger magnitude of χ' observed for the x= 0.65 and 0.5 samples. The changes in exchange interactions distribution are fully attributed to the oxidation of Ni during Li removal as there is no sign of either structural transition or oxidation of Co or Mn.

To further study the role of Ni_{3a}^{2+}, a sample similar to C_3 ($LiNi_{0.65}Co_{0.25}Mn_{0.10}O_2$ post annealed at 1000°C for 12 h (C_3^{PRB})) was produced, see paper VI. A cationic mixing of 12.4% was found using Rietveld refinement of powder XRD data. The XRD was complemented with neutron diffraction experiments [115], which also showed that the rhombohedral structure is stable between 5 and 289 K. At 289 K, a_{hex}=2.8752 Å and

c_{hex}=14.222 Å. The Ni_{3a}^{2+} is accompanied by an additional amount of Ni_{3b}^{2+} in the MO_2-layer and thus a more accurate formula for the material would be: $[Li_{1-x}^{+}Ni_{x}^{2+}]_{3a}[Ni_{0.1+x}^{2+}Ni_{0.55-x}^{3+}Co_{0.25}^{3+}Mn_{0.10}^{4+}]_{3b}O_2$ with x=0.124. In Fig. 3.8, the temperature dependence of the AC and DC susceptibilities are shown. Evidence of a percolating reentrant spin system coexisting with a two dimensional (2D) frustrated spin state in the mid temperature region can be seen and at low enough temperatures the system transforms to a completely frustrated spin state in three dimensions (3D). The experimental results

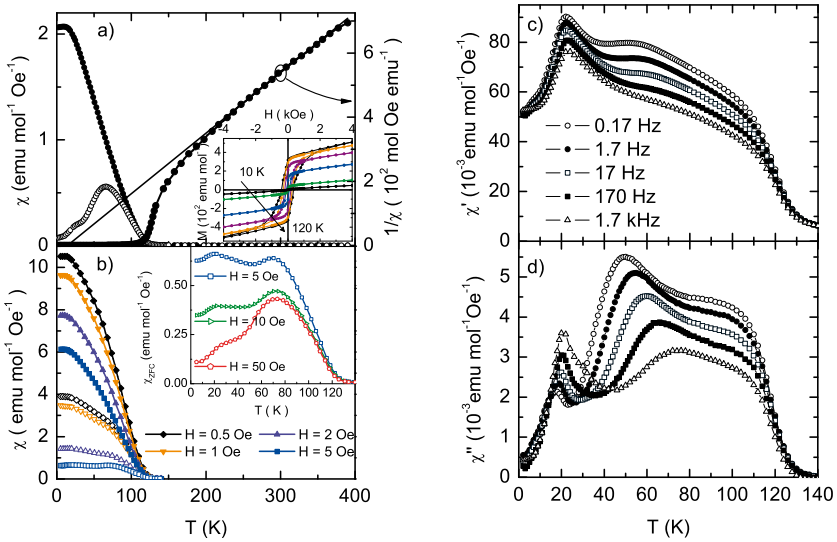

Figure 3.8: **a)** χ_{ZFC} (open symbols) and χ_{FC} (filled symbols) measured at 100 Oe together with the inverse of the susceptibility ($1/\chi_{FC}$) versus temperature. The inset show magnetization versus field at T=10, 20, 35, 60, 100, 120 K **b)** χ_{ZFC}/χ_{FC} susceptibility at different applied fields with the inset showing a zoomed in view of χ_{ZFC} at H=5, 10 and 50 Oe. **c)** in-phase (χ') and **d)** out-of-phase (χ'') susceptibility measured with a h_{ac}= 2 Oe and frequencies between 0.17 and 1700 Hz.

can be explained as follows: the $1/\chi$ curve, seen in Fig. 3.8a, shows an almost textbook like ferrimagnetic behavior with a T_c= 119 K, and from a *CW*-fit θ_w= 14 K and μ_{eff}= 2.38 μ_B/TM were obtained. The occurrence of T_r close to T_c is an indication of a spin cluster system [116]. As concluded from the magnetization versus field results (cf. inset Fig. 3.8a), the clusters are randomly distributed in the material and form a percolating network of magnetic interactions [117, 118]. From neutron powder diffraction data, no extra Bragg peaks (a sign of AF ordering) or intensity increase (a sign of FM ordering) were observed. Thus, the system does not exhibit any long-range translational magnetic ordering. Since magnetometry only yields a bulk

average magnetic response, the observed ferrimagnetic behavior stems from a percolating system, without translational and/or orientational spin order, defined by magnetic interactions of different sign and strength. Notably, the clusters mentioned here are not aggregates of magnetic ions, but rather random percolating entities defined by magnetic exchange interactions. The χ_{ZFC} displays a T_{cusp}= 70 K that is suppressed by an increasing applied magnetic field. The χ'' exhibits a frequency (f) dependent T_{cusp} in the mid temperature region. The magnitude of χ'' increases with decreasing f, indicating a 2D spin frustrated state [8]. For a 2D spin glass, no phase transition is expected at a finite temperature [9] ($T_g \rightarrow 0$), and the spin dynamics follow the generalized Arrhenius law given in Eq. 1.9. The spin freezing temperature (T_f) in the temperature range between 40 to 80 K is identified as T_{cusp} in χ''. A $\tau_{o2}= 5.6\times10^{-13}$ s close to the atomic $\tau_o=10^{-13}$ s [7] and a critical exponent $\psi\nu= 0$ were obtained from scaling analysis and suggest a thermally activated behavior[12]. A 2D spin glass behavior is also seen in the relaxation rate ($S(t)$) and results are discussed later in this text. At even lower temperatures, the second cusp at approximently 23 K is seen in the χ_{ZFC} curve and is distinctly suppressed (more than the T_{cusp}=70 K) as the applied field increases. In this low temperature region the χ'' behavior transforms to a 3D spin glass like behavior [7] such that the magnitude of χ'' increases with increasing frequency. Assuming critical slowing down according to Eq. (1.8) and identifying T_f as the inflection point in the upturn of $\chi''(f)$ after background subtraction, dynamic scaling analysis yields $z\nu$=7.6 corresponding well with results obtained for reentrant [119] and 3D spin glass compounds [7]. The value of $\tau_{o3}= 4.6\times10^{-7}$ s is considerably larger than the atomic spin flip time but similar to values obtained for cluster-glass systems, and accordingly the obtained transition temperature is a cluster glass transition temperature $T_{cg} =$ 17.4 K.

The spin dynamics was further investigated using magnetic relaxation ($m_{ZFC}(t)$) and aging measurements performed on a specially designed RF-SQUID magnetometer [120]. Additionally, the results were analyzed using the ZFC relaxation rate ($S(t)$) given by Eq. (1.10). Changes in $m_{ZFC}(t)$ at each wait time (t_w) show that the spin system is not at equilibrium during the wait time, indicating the spin system is frustrated. As seen in Fig. 3.9a, spin frustration is present at all measured temperatures, and aging persists even up to T_c indicating that clusters of frustrated spins coexist with the ferrimagnetic-like ordering from the onset of spin ordering. The most striking feature is the evolution of $m_{ZFC}(t)$ with measuring temperature (T_m), which is an indication of the development and growth of disordered magnetic clusters with decreasing temperature. The relaxation rate curves are analyzed with respect to their maxima [$S_{max}(t_w)$]. For 3D spin glass and cluster glass systems, S_{max} occurs at $t \approx t_w$ [121], observed in both the high and low temperature regions. 2D spin glasses show a S_{max} at $t \gg t_w$ [122]; this is observed in the mid temperature region for sample C_3^{PRB} (cf.

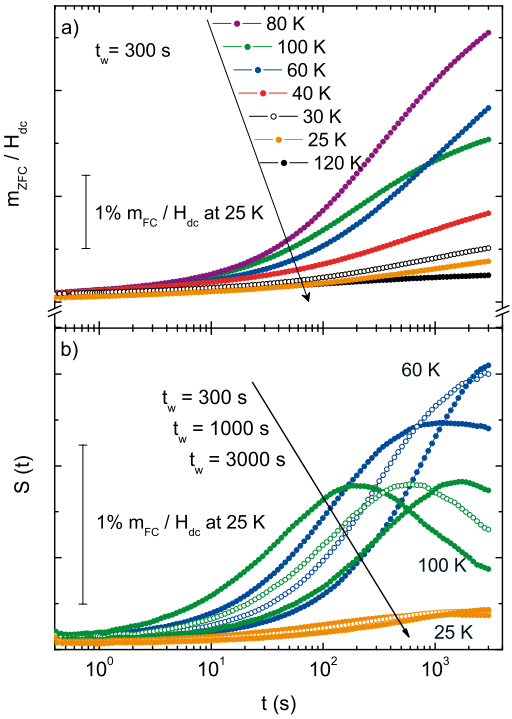

Figure 3.9: **a)** ZFC relaxation of the magnetization m_{ZFC}/H_{dc} versus observation time t at H_{dc} = 0.40 Oe, with t_w= 300 s and different T_m = 25, 30, 40, 60, 80, 100 and 120 K. **b)** Relaxation rate $S(t)$ versus t at 100 K (green), 60 K (blue) and 25 K (orange). H_{dc}=0.40 Oe and t_w= 300, 1000 and 3000 s.

Fig. 3.9b). Defined by the magnitude of the relaxation rate at non-equilibrium and quasi-equilibrium conditions respectively, the ratio $S_{max}/S(t = 1\text{s})$ is very large in the intermediate and high temperature regions in comparison to archetypal 3D spin glass systems. The large $S_{max}/S(t = 1\text{s})$ ratio is a feature previously observed in reentrant systems well above T_g [123], while at the lowest temperatures investigated, the $S_{max}/S(t = 1\text{s})$ ratio is close to values observed for 3D spin glass systems [7].

The results strongly support the proposition that the spin system exhibits a reentrant cluster glass behavior with frustration in 2D and 3D; the behavior conforms well with predictions of the percolating cluster model. The quasi long-range spin order is due to parasitic Ni^{2+}_{3a} inducing 180° AF superexchange interactions of different strengths. Competing AF and FM intralayer interactions in the 3*b*-plane between Ni-Mn, Mn-Mn and Ni-Ni of short range character [105, 106] create the 2D frustrated spin state that coexists with the ferrimagnetic ordering. At low enough temperatures, the 2D frustration as well

as the interlayer interactions are strong enough to enable breakdown of the ferrimagnetic spin order (as described by the random field model [124]) and hence, a completely frustrated spin state in 3D is created.

The compound $LiNi_{0.8}Co_{0.1}Mn_{0.1}O_2$ was heat treated at 900°C for 1 h (C_{811}) discussed in paper V. The time and temperature choosen are those preferred for battery application, as seen in paper VIII. Rietveld refinement of room temperature powder XRD data gave an a_{hex}=2.8721 Å and c_{hex}=14.200 Å and indicated a cationic mixing of 3.9%. The results from AC and DC magnetometry show behavior very similar to the results for sample C_3^{PRB} with the exception that only one T_{cusp}^{ZFC} (at 20 K) is visible and the ferrimagnetic like transition takes place at around 70 K. The *CW*-fit generates a θ_w= -25 K and μ_{eff}= 2.07 μ_B. Non-linear AC susceptibilities of

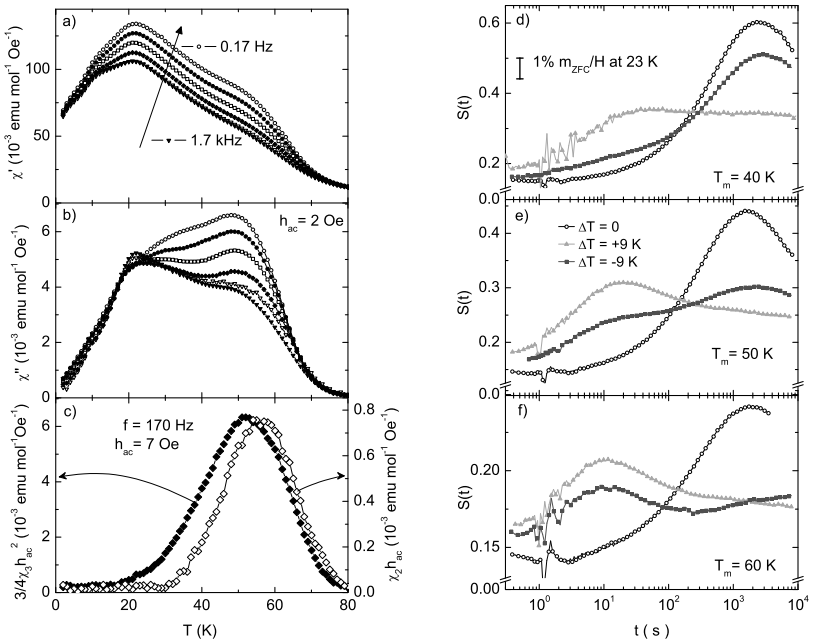

Figure 3.10: **a)** χ' and **b)** χ'' versus temperature (T) for an AC field $h_{ac} = 2$ Oe and frequencies $f = 0.17$, 1.7, 17, 170, 1000 and 1700 Hz. **c)** Second $\chi_2 h_{ac}$ (open diamonds) and third $3/4\chi_3 h_{ac}^2$ (filled diamonds) order non-linear susceptibilities versus T at h_{ac}= 7 Oe and f = 170 Hz. $\chi_2 h_{ac}$ and $3/4\chi_3 h_{ac}^2$ have the same onset temperature, the appearance of different onset temperatures is an artifact due to different y-axis scales. Temperature cycling experiments with $S(t)$ versus t. $\Delta T = 0$, $+9$ and -9 K (open circles, triangles and squares, respectively) with $t_w = 3000$ s and $H = 0.05$ Oe at **d)** $T_m = 40$ K, **e)** $T_m = 50$ K and **f)** $T_m = 60$ K.

second (χ_2) and third (χ_3) order, measured as the second and third harmonic response, respectively, are shown in Fig. 3.10 c. To understand the meaning

of the nonlinear susceptibilies, we consider the generalized expression for the magnetization in the presence of a magnetic field (h);

$$m = m_0 + \chi_1 h + \chi_2 h^2 + \chi_3 h^3 + ..., \tag{3.1}$$

where m_0 is the spontaneous magnetization, χ_1 is the linear susceptibility and χ_2 and χ_3 are the non-linear susceptibilities of 2nd and 3rd order, respectively. The absence of inversion symmetry with respect to the applied field as well as the existence of a non-zero χ_2 at zero applied DC field would be clear evidence of a material with spontaneous magnetization [125]. When a material exhibits spontaneous magnetization and glassy spin dynamics at the same time, both odd and even non-linear susceptibility terms are expected [126, 127]. The results in Fig. 3.10c strongly indicate that the spontaneous magnetization of ferrimagnetic type coexists with a frustrated spin state in the temperature range 30<T<70 K; at lower temperatures complete spin glassiness prevails.

The magnetic relaxation for the C_{811} sample showed similarities to the C_3^{PRB} sample. The main differences lies in the evolution of S_{max}. In the temperature region above 30 K, S_{max} occurs at $t < t_w$ indicating an evolution towards equilibrium that is much faster than in typical spin glasses suggesting that the compound consists of an ordered as well as a frustrated state above 30 K. In sample C_3^{PRB} S_{max} occurs at $t >> t_w$ while in sample C_{811} S_{max} occurs at $t < t_w$, indicating that the 2D frustration is not as pronounced in sample C_{811}. This attributed to fewer intralayer interactions as well as to overshadowing by the onset of ferrimagnetic order. In addition, temperature cycling relaxation experiments have been performed with a second wait time, t_{w2}=100 s. As seen in Fig. 3.10d-e, T_g for the spin system appears to be just below 40 K. Though it was not possible to perform a dynamic scaling analysis, which would provide a glass temperature and critical exponents, the experimental results support the proposal of a percolating system with ferrimagnetic like spin order (T_c= 70 K) coexisting with a 2D frustrated spin state that fully transforms below 40 K to a 3D frustrated state.

The observation of a ferrimagnetic transition is due to magnetic clusters formation defined by 180° superexchange interactions involving Ni_{3a}^{2+}. The ferrimagnetic T_c depends on the magnetic clusters size since larger clusters yield a higher T_c. This is evident when examining the results for sample C_2 and C_{811}, where the latter sample has a lower T_c and a smaller Ni_{3a}^{2+} concentration. The somewhat distorted ferrimagnetic transition, as seen in the $1/\chi$ versus temperature curve, could be due to the appearance of a Mn moment [128, 101, 110] around 60 K. New superexchange interactions would be introduced in the MO_2 layers creating 2D spin frustration, which weakens the ferrimagnetic ordering. The MO_2 frustration is detected in all high concentration Ni_{3a}^{2+} and/or Li deficient samples, and from the measurements on the C_3^{PRB} and C_{811} samples, the magnetic frustration is concluded to exhibit a 2D character. The transition temperature T_g of the 3D spin glass state (seen in all

investigated samples) depends not only on the stoichiometry of the samples but also on the Li deficiency. Between the C_{811} and C_1^{x1} samples there is only a small difference in Ni_{3a}^{2+} concentration (3.9 and 2.8 %, respectively), but a comparatively strong hysteretic magnetic behavior is observed for sample C_{811}, due to Li-deficiency, while sample C_1^{x1} exhibits an almost linear magnetization versus field behavior indicating excess or stoichiometric amounts of Li in the sample [110]. The sample with excess Li exhibits a more homogeneous distribution of TM-ions in the MO_2 slab. The non magnetic Co^{3+} dilutes the magnetic structure and helps to break up the ferrimagnetic clusters while Li-deficientcy induces a more disordered transition metal distribution resulting in both larger clusters and higher degree of spin frustration. To reiterate, the clusters mentioned here are not aggregates of magnetic ions but rather entities defined by the magnetic exchange interactions. A low temperature paramagnetic behavior indicates a stoichiometric amount of Li, small cationic mixing and more homogeneously distributed TM-ions throughout the whole compound; a plausible conclusion is that the lower the temperature is for onset of spin ordering, the better the material is as a cathode in battery applications.

Svensk sammanfattning

Magnetism har länge fascinerat människan med den första kända nedteckningen om magnetism gjord av Thales från Miletos (625−545 f.Kr.). Människans teknologiska framsteg har alltid varit nära relaterad till magnetism, från sjöfarares användning av magnetit till kompasser via upptäckten av elektromagnetismen till dagens elektronik som, troligtvis, inom en snar framtid kommer att var helt magnetbaserade.

Spinntronik

Dagens elektroniska komponenter baseras på elektronens laddning, medan elektronens spinn, tills helt nyligen, nästan helt har ignorerats. Genom att lägga till spinnets frihetsgrader öppnar man upp för nya komponenter som kombinerar konventionell mikroelektronik med spinn-baserade effekter, vilka kommer från växelverkan mellan laddningsbärarens spinn och materialets magnetiska egenskaper. Den nya teknologin går under namnet Spinntronik (spinn-transport-elektronik) och öppnar upp möjligheter att få beständiga minnen, ökad dataprocesshastighet, minskad elkonsumtion och ökad datalagringskapacitet jämfört med dagens konventionella halvledarkomponenter. Den främsta drivande kraften bakom Spinntroniken är farhågorna att processorutvecklingen, med dagens teknologi, kommer att avstanna. Det vill säga att vi kommer att få uppleva ett avbrott i Moore's lag som säger att antalet transistorer på ett data chip fördubblas var 24:e månad.

En väg till förverkligande av Spinntronik vore att dopa en känd halvledare med små koncentrationer av magnetiska joner och därigenom få ett material som har både halvledaregenskaper och som är ferromagnetiskt.

I denna avhandling har zink-oxid (ZnO) dopats med övergångsmetaller för att försöka skapa en ferromagnetiskt halvledare. Våra resultat visar att det magnetiska beteendet har sitt ursprung i utfällningar av nanopartiklar och/eller sekundära faser. Storleken på partiklarna är så små att de är svåra att upptäcka med även högupplöst röntgendiffraktion och transmissions-elektronmikroskopi. Dock kan partikelstorleken vara tillräcklig för att generera ett tillräckligt stort spontant magnetiskt moment vid rumstemperatur som lätt kan förväxlas med intrinsisk ferromagnetism.

En alternativ metod är att injicera en spinnpolariserad ström, med hjälp av en ferromagnetisk metal som kontaktmaterial, in i en vanlig halvledare där elektronens precession bestäms av grindspänningen om elektronen skall anlända som spinn-upp eller spinn-ner i ledningskontakten. Kraven för ett sådant material skulle vara att det är ferromagnetiskt över rumstemperatur samt att det har god gitteranpassning, dvs atomavstånden i kontaktmaterialet och halvledaren skall vara likvärdiga. Ett sådant magnetiskt kontakt material är manganarsenid (MnAs), eftersom MnAs kan deponeras på en vanlig halvledare som kisel (Si) eller galliumarsenid (GaAs) med bibehållen epitaxi (dvs med hög gitteranpassning) och MnAs har en ferromagnetisk övergångstemperatur (T_c) strax över rumstemperatur, 40°C. MnAs har en stark magnetisk anisotropi, där det magnetiska svaret varierar beroende på magnetfältets riktning, och uppvisar en strukturell fasövergång tillsammans med den magnetiska fasövergången från ett ferromagnetisk hexagonalt till ett paramagnetiskt ortorhombiskt gitter. Enligt våra mätningar på tunna filmer av MnAs växta på GaAs(100) substrat, ses ett förhöjt magnetiskt moment och en ökad magnetisk anisotropi jämfört med bulk MnAs och tidigare publicerade resultat på tunna filmer. De förändrade magnetiska beteendet härrör från stora lokala töjningar i gittret med en tendens till ökat T_c med kortare hexagonal c-axel. Töjningarna skapas under kristalltillväxten och våra resultat visar på möjligheterna att finjustera de magnetiska egenskaperna under tillverkningen för att få önskvärda parametrar.

Magnetisk frustration i oxider

Magnetisk frustration uppstår när flera (magnetiska) utbytesväxelverkningar inte kan uppfyllas samtidigt. Spinnen fluktuerar mellan olika tillstånd och upplinjeringen av momenten får inte någon struktur och blir oordnad som atomernas positioner i glas, därav namnet spinn-glas. Ett spinnglas beteende uppstår när ett system innehåller konkurrerande ferro- och antiferromagnetiska utbytesvävelverkningar, som gärna kan vara olika starka. Om ett material innehåller en övergångsmetall med blandad valens, exempelvis Mn^{3+} och Mn^{4+}, kan det ge upphov till olika utbytesvävelverkningar. Om materialet dessutom innehåller en triangulär struktur, innehållande syre atomer (O), har vi skapat en god grogrund för magnetisk frustration. Då det inte är möjligt att samtidigt uppfylla olika växelverkningarna kommer det magnetiska systemet inte nå jämvikt inom överskådlig tid och magnetiseringen kommer att förändras med tiden, kallat magnetisk åldring. Magnetisk åldring är olika för olika temperaturer och väldigt känslig för provets historia med avseende på temperatur och magnetfält.

Dubbelperovskiten, $SrMnWO_6$, har ett antiferromagnetiskt grundtillstånd men med dopning med trevärt lantan (La^{3+}) fås ett spinnglas likt tillstånd

vid låga temperaturer ($-263°C$). Det beror på att strontium är tvåvärt (Sr^{2+}) och en del av de sexvärda volfram jonerna (W^{6+}) reduceras till femvärda (W^{5+}) joner. En ferromagnetisk växelverkan kommer nu att uppstå då W^{5+} växelverkar med Mn^{2+} och ett frustrerat system med antiferro- och ferromagnetiska växelverkningar har därmed skapats. Med högre La^{3+} dopning ökar frustrationen med fler konkurrerande växelverkningar och temperaturen för då $(Sr,La)MnWO_6$ blir frustrerat, den så kallade spinnglas temperaturen (T_g), kommer att öka.

I dagens Li-jon batteri används $LiCoO_2$ som katodmaterial. Dock strävar man efter att byta ut kobolt mot billigare och miljövänligare övergångsmetaller men samtidigt behålla den fördelaktiga strukturen samt öka mobiliteten av Li-jonerna i materialet. I de nyaste batterierna används $LiNi_{1/3}Co_{1/3}Mn_{1/3}O_2$ utan någon uppenbar anledning till varför man valt just denna sammansättning. Då övergångsmetallerna kommer att ha olika magnetisk växelverkan beroende på var och hur de sitter i kristallstrukturen kan en mätning av de magnetiska egenskaperna ge ett svar på provets stökiometriska sammansättning. Känsligheten i magnetiska mätningar med en SQUID[4] sensor är väldigt hög och det är därför möjligt att detektera mycket små koncentrationer av föroreningar. Vi har undersökt $LiNi_xCo_yMn_zO_2$ med x= 0,8/0,65 , y = 0,25/0,1 , z=0,1 och som dessutom utsatts för olika värmebehandlingar. För små koncentrationer av Ni^{2+} i Li-lagret, så kallad katjon mixing (den vanligaste deffekten vid Li-katod tillverkning), ses ett spinnglas likt beteende vid temperaturer runt 7° över absoluta nollpunkten och för större katjon mixing ($>2\%$) uppstår en ferrimagnetisk ordning runt $-183°C$. Vad mer intressant är, för dåliga batteri material med hög katjon mixing uppträder ett frustrerat system vid höga temperaturer ($-213°C$) som först är frustrerat i två dimensioner för att med sjunkande temperatur bli frustrerat i tre dimensioner. Detta komplicerade magnetiska beteende tros härröra från magnetiska växelverkningar som uppstår på grund av katjon mixing och förekomsten av Mn i materialet.

Exemplet ovan visar hur magnetisk grundforskning kan bli direkt applicerbar på och ge värdefull återkoppling till kommersiellt inriktad forskning med direkta applikationer.

[4]SQUID - superconducting quantum interference device, samma sensor som exempelvis används vid magnetoencefalografi vilket innebär undersökning av hjärnans olika funktioner.

Acknowledgements

To Peter, my advisor, for always being positive, showing support and understanding both professionally as well as in private. For patiently listening, answering and never being judgemental. For being a friend.
To my co-advisors Per and Klas, for answering any question, discussing any issue, always with a smile. To Matthias for helping a person with whatever, whenever. A true friend to all of us. To my coworkers; Rebecca, Roland and former Peter Warnicke. All of you make up a great group who make me wanna get up early every morning (even mondays) and go to work.

To my main collaborators Charlie and Ronny for providing a positive environment, always a good laugh. To the rest of my collaborators, thanks to Torbjörn and Kristina, Ottosson and Annika, Mohammed, Kenza, Ismael, Diana, Anders, Maggan, Auregane, Sumanta, Olle, Biplab and Victoria Coleman, it was great working with you. To my friends at work; the grannies on level 4 (a.k.a. Pia and Malin, we all know what you look like when you have aged) for providing a confy chair in which to share ones thoughts, Annika, Zareh, Shuyi, To C-G for forcing me sharpening my arguments and all the rest of the people at the Solid State Physics, Mattias and Teresa at Ångström×10 group, Panos and Masoud at Materials Physics.

A big thanks to Anna Maria Lundins Stipendiefond at Smålands Nation for 7 issued travel grants.

The reader should thank Victoria Sternhagen for correcting my English in this thesis and for taking away all the run-on sentences and prepositions stacked upon preposition, upon preposition, upon preposition... in short for making the reading of this thesis an enjoyable and not a frantic moment searching for the verb. I thank her for her patience while doing it.

Finally, to Sebastian and Victoria for your love, your patience and understanding, your challenges and questioning, your affection and care, for teaching me all about the most important things in life...

Thank you all - for the best time of my life.

Bibliography

[1] W. Gillbert, *De Magnete*. 1600.

[2] R. Feynman, *The Feynman Lectures in Physics*, vol. 2. Addison-Wesley Professional, 1964.

[3] M. V. Berry and A. K. Geim, "Of flying frogs and levitrons," *European Journal of Physics*, vol. 18, p. 307, 1997.

[4] J. Kanamori, "Superexchange interaction and symmetry properties of electron orbitals," *Journal of Physics and Chemistry of Solids*, vol. 10, no. 2-3, pp. 87 – 98, 1959.

[5] J. B. Goodenough, *Magnetism and The Chemical Bond*. Interscience, New York, 1963.

[6] R. Skomski, *Simple Models of Magnetism*. Oxford University Press, USA, 2008.

[7] P. Svedlindh, P. Granberg, P. Nordblad, L. Lundgren, and H. S. Chen, "Relaxation in spin glasses at weak magnetic fields," *Physical Review B*, vol. 35, pp. 268–273, Jan 1987.

[8] C. Dekker, A. F. M. Arts, H. W. de Wijn, A. J. van Duyneveldt, and J. A. Mydosh, "Activated dynamics in a two-dimensional Ising spin glass: $Rb_2Cu_{1-x}Co_xF_4$," *Physical Review B*, vol. 40, pp. 11243–11251, Dec 1989.

[9] P. Granberg, P. Nordblad, P. Svedlindh, L. Lundgren, R. Stubi, G. G. Kenning, D. L. Leslie-Pelecky, J. Bass, and J. Cowen, "Dimensionality crossover in CuMn spin-glass films," *Journal of Applied Physics*, vol. 67, no. 9, pp. 5252–5254, 1990.

[10] D. S. Fisher and D. A. Huse, "Static and dynamic behavior of spin-glass films," *Physical Review B*, vol. 36, pp. 8937–8940, Dec 1987.

[11] C. Djurberg, J. Mattsson, P. Nordblad, L. Hoines, and J. A. Cowen, "2d dynamic exponent derived from CuMn spin glass films," *Journal of Magnetism and Magnetic Materials*, vol. 140-144, no. Part 3, pp. 1721 – 1722, 1995. International Conference on Magnetism.

[12] R. Mathieu and Y. Tokura, "The Nanoscale Phase Separation in Hole-Doped Manganites," *Journal of the Physical Society of Japan*, vol. 76, no. 12, p. 124706, 2007.

[13] T. Jonsson, K. Jonason, P. Jönsson, and P. Nordblad, "Nonequilibrium dynamics in a three-dimensional spin glass," *Physical Review B*, vol. 59, pp. 8770–8777, Apr 1999.

[14] R. Mathieu, P. Nordblad, D. N. H. Nam, N. X. Phuc, and N. V. Khiem, "Short-range ferromagnetism and spin-glass state in $Y_{0.7}Ca_{0.3}MnO_3$," *Physical Review B*, vol. 63, p. 174405, Mar 2001.

[15] *http://www.intel.com/technology/mooreslaw/*.

[16] S. A. Wolf, A. Y. Chtchelkanova, and D. M. Treger, "Spintronics - A retrospective and perspective," *IBM Journal of Research and Development*, vol. 50, pp. 101 –110, 2006.

[17] I. Žutić, J. Fabian, and S. Das Sarma, "Spintronics: Fundamentals and applications," *Reviews of Modern Physics*, vol. 76, no. 2, pp. 323–410, 2004.

[18] S. A. Wolf, D. D. Awschalom, R. A. Buhrman, J. M. Daughton, S. von Molnar, M. L. Roukes, A. Y. Chtchelkanova, and D. M. Treger, "Spintronics: A Spin-Based Electronics Vision for the Future," *Science*, vol. 294, no. 5546, pp. 1488–1495, 2001.

[19] M. N. Baibich, J. M. Broto, A. Fert, F. N. Van Dau, F. Petroff, P. Etienne, G. Creuzet, A. Friederich, and J. Chazelas, "Giant magnetoresistance of (001)Fe/(001)Cr Magnetic Superlattices," *Physical Review Letters*, vol. 61, pp. 2472–2475, 1988.

[20] G. Binasch, P. Grünberg, F. Saurenbach, and W. Zinn, "Enhanced magnetoresistance in layered magnetic structures with antiferromagnetic interlayer exchange," *Physical Review B*, vol. 39, pp. 4828–4830, 1989.

[21] S. Bader and S. Parkin, "Spintronics," *Annual Review of Condensed Matter Physics*, vol. 1, pp. 71–88, 2010.

[22] S. Datta and B. Das, "Electronic analog of the electro-optic modulator," *Applied Physics Letters*, vol. 56, pp. 665–667, 1990.

[23] H. Ohno, A. Shen, F. Matsukura, A. Oiwa, A. Endo, S. Katsumoto, and Y. Iye, "(Ga,Mn)As: A new diluted magnetic semiconductor based on GaAs," *Applied Physics Letters*, vol. 69, pp. 363–365, 1996.

[24] K. Olejník, M. H. S. Owen, V. Novák, J. Mašek, A. C. Irvine, J. Wunderlich, and T. Jungwirth, "Enhanced annealing, high Curie temperature, and low-voltage gating in (Ga,Mn)As: A surface oxide control study," *Physical Review B*, vol. 78, p. 054403, 2008.

[25] T. Dietl, H. Ohno, F. Matsukura, J. Cibert, and D. Ferrand, "Zener Model Description of Ferromagnetism in Zinc-Blende Magnetic Semiconductors," *Science*, vol. 287, pp. 1019–1022, 2000.

[26] M. H. Huang, S. Mao, H. Feick, H. Yan, Y. Wu, H. Kind, E. Weber, R. Russo, and P. Yang, "Room-Temperature Ultraviolet Nanowire Nanolasers," *Science*, vol. 292, p. 5523, 2001.

[27] M. Kroutvar, Y. Ducommun, D. Heiss, M. Bichler, D. Schuh, G. Abstreiter, and J. J. Finley, "Optically programmable electron spin memory using semiconductor quantum dots," *Nature*, vol. 432, pp. 81–84, Nov. 2004.

[28] S. J. Pearton, D. P. Norton, K. Ip, Y. W. Heo, and T. Steiner, "Recent progress in processing and properties of ZnO," *Progress in Materials Science*, vol. 50, pp. 293 – 340, 2005.

[29] U. Özgür, Y. I. Alivov, C. Liu, A. Teke, M. A. Reshchikov, S. Doğan, V. Avrutin, S.-J. Cho, and H. Morkoç, "A comprehensive review of ZnO materials and devices," *Journal of Applied Physics*, vol. 98, p. 041301, 2005.

[30] K. Momma and F. Izumi, "*VESTA*: a three-dimensional visualization system for electronic and structural analysis," *Journal of Applied Crystallography*, vol. 41, pp. 653–658, 2008.

[31] C. H. Bates, W. B. White, and R. Roy, "The solubility of transition metal oxides in zinc oxide and the reflectance spectra of Mn^{2+} and Fe^{2+} in tetrahedral fields," *Journal of Inorganic and Nuclear Chemistry*, vol. 28, pp. 397–405, 1966.

[32] T. Fukumura, Z. Jin, A. Ohtomo, H. Koinuma, and M. Kawasaki, "An oxide-diluted magnetic semiconductor: Mn-doped ZnO," *Applied Physics Letters*, vol. 75, pp. 3366–3368, 1999.

[33] S. Kolesnik, B. Dabrowski, and J. Mais, "Origin of Spin-Glass Behavior of $Zn_{1-x}Mn_xO$," *Journal of Superconductivity*, vol. 15, pp. 251–255, 2002.

[34] P. Sharma, A. Gupta, K. V. Rao, F. J. Owens, R. Sharma, R. Ahuja, J. M. O. Guillen, B. Johansson, and G. A. Gehring, "Ferromagnetism above room temperature in bulk and transparent thin films of Mn-doped ZnO," *Nature Materials*, vol. 2, pp. 673 – 677, 2003.

[35] A. Flodström, "det största som hänt sedan transistorn uppfanns," *Svenska Dagbladet*, September 23rd, 2003.

[36] R. Seshadri, "Zinc oxide-based diluted magnetic semiconductors," *Current Opinion in Solid State and Materials Science*, vol. 9, pp. 1–7, 2005.

[37] D. Iuşan, B. Sanyal, and O. Eriksson, "Theoretical study of the magnetism of Mn-doped ZnO with and without defects," *Physical Review B*, vol. 74, p. 235208, 2006.

[38] C. D. Pemmaraju, R. Hanafin, T. Archer, H. B. Braun, and S. Sanvito, "Impurity-ion pair induced high-temperature ferromagnetism in Co-doped ZnO," *Physical Review B*, vol. 78, p. 054428, 2008.

[39] K. Sato and H. Katayama-Yoshida, "Material Design for Transparent Ferromagnets with ZnO-Based Magnetic Semiconductors," *Japanese Journal of Applied Physics*, vol. 39, pp. L555–L558, 2000.

[40] K. Ueda, H. Tabata, and T. Kawai, "Magnetic and electric properties of transition-metal-doped ZnO films," *Applied Physics Letters*, vol. 79, pp. 988–990, 2001.

[41] S. A. Chambers, "Ferromagnetism in doped thin-film oxide and nitride semiconductors and dielectrics," *Surface Science Reports*, vol. 61, pp. 345–381, 2006.

[42] J. Coey, "Dilute magnetic oxides," *Current Opinion in Solid State and Materials Science*, vol. 10, pp. 83 – 92, 2006.

[43] K. R. Kittilstved, W. K. Liu, and D. R. Gamelin, "Electronic structure origins of polarity-dependent high-T_c ferromagnetism in oxide-diluted magnetic semiconductors," *Nature Materials*, vol. 5, pp. 291 – 297, 2006.

[44] L. Néel, "Magnétisme - Superparamagnétisme des grains très fins antiferromagnétiques," *Comptes Rendus Hebdomadaires des Seances de l'Academie des Sciences*, vol. 252, p. 4075, 1961.

[45] T. Dietl, T. Andrearczyk, A. Lipinska, M. Kiecana, M. Tay, and Y. Wu, "Origin of ferromagnetism in $Zn_{1-x}Co_xO$ from magnetization and spin-dependent magnetoresistance measurements," *Physical Review B*, vol. 76, p. 155312, 2007.

[46] K. N. Hutchings, M. Wilson, P. A. Larsen, and R. A. Cutler, "Kinetic and thermodynamic considerations for oxygen absorption/desorption using cobalt oxide," *Solid State Ionics*, vol. 177, pp. 45 – 51, 2006.

[47] A. Quesada, M. A. García, M. Andrés, A. Hernando, J. F. Fernández, A. C. Caballero, M. S. Martín-González, and F. Briones, "Ferromagnetism in bulk Co-Zn-O," *Journal of Applied Physics*, vol. 100, p. 113909, 2006.

[48] H. J. Kim, I. C. Song, J. H. Sim, H. Kim, D. Kim, Y. E. Ihm, and W. K. Choo, "Growth and characterization of spinel-type magnetic semiconductor $ZnCo_2O_4$ by reactive magnetron sputtering," *Physica Status Solidi (b)*, vol. 241, p. 1553–1556, 2004.

[49] D. Iuşan, M. Kabir, O. Grånäs, O. Eriksson, and B. Sanyal, "Microscopic picture of Co clustering in ZnO," *Physical Review B*, vol. 79, p. 125202, 2009.

[50] *private communication, R. Allenspach, IBM Research, Rüschlikon, CH.*

[51] G. Schmidt, D. Ferrand, L. W. Molenkamp, A. T. Filip, and B. J. van Wees, "Fundamental obstacle for electrical spin injection from a ferromagnetic metal into a diffusive semiconductor," *Physical Review B*, vol. 62, pp. R4790–R4793, Aug 2000.

[52] E. I. Rashba, "Theory of electrical spin injection: Tunnel contacts as a solution of the conductivity mismatch problem," *Physical Review B*, vol. 62, pp. R16267–R16270, Dec 2000.

[53] K. Akeura, M. Tanaka, M. Ueki, and T. Nishinaga, "Epitaxial ferromagnetic MnAs thin films grown by molecular beam epitaxy on Si (001) substrates," *Applied Physics Letters*, vol. 67, no. 22, pp. 3349–3351, 1995.

[54] L. Däweritz, "Interplay of stress and magnetic properties in epitaxial MnAs films," *Reports on Progress in Physics*, vol. 69, p. 2581, 2006.

[55] K. H. Ploog, "Spin injection in ferromagnet-semiconductor heterostructures at room temperature (invited)," *Journal of Applied Physics*, vol. 91, no. 10, pp. 7256–7260, 2002.

[56] F. Heusler, "Über Manganbronze und über die Synthese magnetisierbarer Legierungen aus unmagnetischen Metallen," *Zeitschrift Angewandte Chemie*, vol. 17, pp. 260–264, 1904.

[57] S. Hilpert and T. Dieckmann, "Über Arsenide. I. (Eisen- und Manganarsenide.)," *Berichte der deutschen chemischen Gesellschaft*, vol. 44, p. 2378–2385, 1911.

[58] B. T. M. Willis and H. P. Rooksby, "Magnetic Transitions and Structural Changes in Hexagonal Manganese Compounds," *Proceedings of the Physical Society*, vol. B67, p. 290, 1954.

[59] L. F. Bates, "The Specific Heats of Ferromagnetic Substances," *Proceedings of the Royal Society (London)*, vol. A117, pp. 680–691, 1928.

[60] O. Beckman and L. Lundgren, "Compounds of transition elements with nonmetals," vol. 6 of *Handbook of Magnetic Materials*, ch. 3, pp. 181 – 287, Elsevier Science Publiching Company Inc., 1991.

[61] H. Ido, "Magnetic properties of mixed crystals with NiAs-type structure," *Journal of Applied Physics*, vol. 57, pp. 3247–3249, 1985.

[62] R. W. De Blois and D. S. Rodbell, "Magnetic First-Order Phase Transition in Single-Crystal MnAs," *Physical Review*, vol. 130, pp. 1347–1360, May 1963.

[63] C. Guillaud, "Les points de transformation des composés définis MnAs, MnBi en relation avec un mécanisme probable d'antiferromagnétisme," *Journal de Physique et Le Radium*, vol. 12, pp. 223 – 227, 1951.

[64] C. Kittel, "Model of Exchange-Inversion Magnetization," *Physical Review*, vol. 120, pp. 335–342, Oct 1960.

[65] G. E. Bacon and R. Street, "Magnetic Structure of Manganese Arsenide," *Nature*, vol. 175, pp. 518–518, 1955.

[66] C. P. Bean and D. S. Rodbell, "Magnetic Disorder as a First-Order Phase Transformation," *Physical Review*, vol. 126, pp. 104–115, Apr 1962.

[67] I. Rungger and S. Sanvito, "Ab initio study of the magnetostructural properties of MnAs," *Physical Review B*, vol. 74, p. 024429, Jul 2006.

[68] M. K. Niranjan, B. R. Sahu, and L. Kleinman, "Density functional determination of the magnetic state of β-MnAs," *Physical Review B*, vol. 70, p. 180406, Nov 2004.

[69] H. Yamaguchi, A. K. Das, A. Ney, T. Hesjedal, C. Pampuch, D. M. Schaadt, and R. Koch, "From ferro- to antiferromagnetism via exchange-striction of MnAs/GaAs(001)," *Europhysics Letters*, vol. 72, p. 479, 2005.

[70] J. B. Goodenough and J. A. Kafalas, "High-Pressure Study of the First-Order Phase Transition in MnAs," *Physical Review*, vol. 157, pp. 389–395, May 1967.

[71] N. Menyuk, J. A. Kafalas, K. Dwight, and J. B. Goodenough, "Effects of Pressure on the Magnetic Properties of MnAs," *Physical Review*, vol. 177, pp. 942–951, 1969.

[72] A. Zieba, R. Zach, H. Fjellvåg, and A. Kjekshus, "Effect of external pressure and chemical substitution on the phase transitions in MnAs," *Journal of Physics and Chemistry of Solids*, vol. 48, no. 1, pp. 79 – 89, 1987.

[73] C. Kuhrt, T. Schittny, and K. Bärner, "Magnetic B–T Phase Diagram of Anion Substituted MnAs. Magnetocaloric Experiments," *Physica Status Solidi (a)*, vol. 91, p. 105–113, 1985.

[74] H. Wada and Y. Tanabe, "Giant magnetocaloric effect of $MnAs_{1-x}Sb_x$," *Applied Physics Letters*, vol. 79, no. 20, pp. 3302–3304, 2001.

[75] D. H. Mosca, F. Vidal, and V. H. Etgens, "Strain Engineering of the Magnetocaloric Effect in MnAs Epilayers," *Physical Review Letters*, vol. 101, p. 125503, Sep 2008.

[76] F. Iikawa, M. J. S. P. Brasil, O. D. D. Couto, C. Adriano, C. Giles, and L. Däweritz, "Effect of MnAs/GaAs(001) film accommodations on the phase-transition temperature," *Applied Physics Letters*, vol. 85, no. 12, pp. 2250–2252, 2004.

[77] F. Iikawa, M. J. S. P. Brasil, C. Adriano, O. D. D. Couto, C. Giles, P. V. Santos, L. Däweritz, I. Rungger, and S. Sanvito, "Lattice Distortion Effects on the Magnetostructural Phase Transition of MnAs," *Physical Review Letters*, vol. 95, p. 077203, Aug 2005.

[78] A. K. Das, C. Pampuch, A. Ney, T. Hesjedal, L. Däweritz, R. Koch, and K. H. Ploog, "Ferromagnetism of MnAs Studied by Heteroepitaxial Films on GaAs(001)," *Physical Review Letters*, vol. 91, p. 087203, Aug 2003.

[79] P. M. Oppeneer, V. N. Antonov, T. Kraft, H. Eschrig, A. N. Yaresko, and A. Y. Perlov, "First-principles study of the giant magneto-optical Kerr effect in MnBi and related compounds," *Journal of Applied Physics*, vol. 80, no. 2, pp. 1099–1105, 1996.

[80] K. Katoh, A. Yanase, and K. Motizuki, "Electronic band structures of NiAs-type transition metal compounds," *Journal of Magnetism and Magnetic Materials*, vol. 54-57, no. Part 2, pp. 959 – 960, 1986.

[81] S. Sanvito and N. A. Hill, "Ground state of half-metallic zinc-blende MnAs," *Physical Review B*, vol. 62, pp. 15553–15560, Dec 2000.

[82] J.-P. Bouchaud, V. Dupuis, J. Hammann, and E. Vincent, "Separation of time and length scales in spin glasses: Temperature as a microscope," *Physical Review B*, vol. 65, p. 024439, Dec 2001.

[83] J. A. Mydosh, "Disordered magnetism and spin glasses," *Journal of Magnetism and Magnetic Materials*, vol. 157-158, pp. 606 – 610, 1996. European Magnetic Materials and Applications Conference.

[84] P. Nordblad, "Minne, åldring och pånyttfödelse; karaktärsdrag hos spinnglas," *Kosmos*, pp. 121 – 130, 2010.

[85] A. P. Ramirez, "Strongly Geometrically Frustrated Magnets," *Annual Review of Materials Science*, vol. 24, no. 1, pp. 453–480, 1994.

[86] C. Castelnovo, R. Moessner, and S. L. Sondhi, "Magnetic monopoles in spin ice," *Nature*, vol. 451, pp. 42–45, Jan. 2008.

[87] D. J. P. Morris, D. A. Tennant, S. A. Grigera, B. Klemke, C. Castelnovo, R. Moessner, C. Czternasty, M. Meissner, K. C. Rule, J.-U. Hoffmann, K. Kiefer, S. Gerischer, D. Slobinsky, and R. S. Perry, "Dirac Strings and Magnetic Monopoles in the Spin Ice $Dy_2Ti_2O_7$," *Science*, vol. 326, no. 5951, pp. 411–414, 2009.

[88] S. T. Bramwell, S. R. Giblin, S. Calder, R. Aldus, D. Prabhakaran, and T. Fennell, "Measurement of the charge and current of magnetic monopoles in spin ice," *Nature*, vol. 461, pp. 956–959, Oct. 2009.

[89] S. Ladak, D. E. Read, G. K. Perkins, L. F. Cohen, and W. R. Branford, "Direct observation of magnetic monopole defects in an artificial spin-ice system," *Nature Physics*, vol. 6, pp. 359–363, May 2010.

[90] A. Schumann, B. Sothmann, P. Szary, and H. Zabel, "Charge ordering of magnetic dipoles in artificial honeycomb patterns," *Applied Physics Letters*, vol. 97, no. 2, p. 022509, 2010.

[91] Ruhr-Universitaet-Bochum, "Spin Ice Used to Examine Exotic Properties of Magnetic Systems.," *Science Daily*, vol. 9, September 2010.

[92] J. M. D. Coey, M. Viret, and S. von Molnaacuter, "Mixed-valence manganites," *Advances in Physics*, vol. 48, pp. 167 – 293, 1999.

[93] M. K. Wu, J. R. Ashburn, C. J. Torng, P. H. Hor, R. L. Meng, L. Gao, Z. J. Huang, Y. Q. Wang, and C. W. Chu, "Superconductivity at 93 K in a new mixed-phase Y-Ba-Cu-O compound system at ambient pressure," *Physical Review Letters*, vol. 58, pp. 908–910, Mar 1987.

[94] K.-I. Kobayashi, T. Kimura, H. Sawada, K. Terakura, and Y. Tokura, "Room-temperature magnetoresistance in an oxide material with an ordered double-perovskite structure," *Nature*, vol. 395, pp. 677–680, Oct. 1998.

[95] J. Rodríguez-Carvajal, "Recent advances in magnetic structure determination by neutron powder diffraction," *Physica B: Condensed Matter*, vol. 192, no. 1-2, pp. 55 – 69, 1993.

[96] Q. Lin, M. Greenblatt, and M. Croft, "Evolution of structure and magnetic properties in electron-doped double perovskites, $Sr_{2-x}La_xMnWO_6$ ($0 \leq x \leq 1$)," *Journal of Solid State Chemistry*, vol. 178, no. 5, pp. 1356 – 1366, 2005.

[97] A. K. Azad, S. Ivanov, S. G. Eriksson, H. Rundlöf, J. Eriksen, R. Mathieu, and P. Svedlindh, "Structural and magnetic properties of the double perovskite Sr_2MnWo_6," *Journal of Magnetism and Magnetic Materials*, vol. 237, no. 2, pp. 124 – 134, 2001.

[98] S.-H. Lee, H. Kikuchi, Y. Qiu, B. Lake, Q. Huang, K. Habicht, and K. Kiefer, "Quantum-spin-liquid states in the two-dimensional kagome antiferromagnets $Zn_xCu_{4-x}(OD)_6Cl_2$," *Nature Materials*, vol. 6, pp. 853–857, Nov. 2007.

[99] P. Fazekas and P. W. Anderson, "On the ground state properties of the anisotropic triangular antiferromagnet," *Philosophical Magazine*, vol. 30, pp. 423 – 440, 1974.

[100] K. Hirakawa, H. Kadowaki, and K. Ubukoshi, "Experimental studies of triangular lattice antiferromagnets with $S = 1/2$: $NaTiO_2$ and $LiNiO_2$," *Journal of the Physical Society of Japan*, vol. 54, no. 9, pp. 3526–3536, 1985.

[101] N. A. Chernova, M. Ma, J. Xiao, M. S. Whittingham, J. Breger, and C. P. Grey, "Layered $Li_xNi_yMn_yCo_{1-2y}O_2$ Cathodes for Lithium Ion Batteries: Understanding Local Structure via Magnetic Properties," *Chemistry of Materials*, vol. 19, no. 19, pp. 4682–4693, 2007.

[102] M. Núñez Regueiro, E. Chappel, G. Chouteau, and C. Delmas, "Magnetic structure of $Li_{1-x}Ni_{1+x}O_2$," *The European Physical Journal B - Condensed Matter and Complex Systems*, vol. 16, pp. 37–41, 2000. 10.1007/s100510070246.

[103] E. Chappel, M. D. Núñez Regueiro, S. de Brion, G. Chouteau, V. Bianchi, D. Caurant, and N. Baffier, "Interlayer magnetic frustration in quasistoichiometric $Li_{1-x}Ni_{1+x}O_2$," *Physical Review B*, vol. 66, p. 132412, Oct 2002.

[104] M. J. Lewis, B. D. Gaulin, L. Filion, C. Kallin, A. J. Berlinsky, H. A. Dabkowska, Y. Qiu, and J. R. D. Copley, "Ordering and spin waves in $NaNiO_2$: A stacked quantum ferromagnet," *Physical Review B*, vol. 72, p. 014408, Jul 2005.

[105] J. Sugiyama, Y. Ikedo, K. Mukai, J. H. Brewer, E. J. Ansaldo, G. D. Morris, K. H. Chow, H. Yoshida, and Z. Hiroi, "Incommensurate magnetic order in Ag_2NiO_2 studied with muon-spin-rotation and relaxation spectroscopy," *Physical Review B*, vol. 73, p. 224437, Jun 2006.

[106] J. Sugiyama, K. Mukai, Y. Ikedo, P. L. Russo, H. Nozaki, D. Andreica, A. Amato, K. Ariyoshi, and T. Ohzuku, "Static magnetic order in the triangular lattice of Li_xNio_2 $(x \leq 1)$: Muon-spin spectroscopy measurements," *Physical Review B*, vol. 78, p. 144412, Oct 2008.

[107] M. S. Whittingham, "The Role of Ternary Phases in Cathode Reactions," *Journal of The Electrochemical Society*, vol. 123, no. 3, pp. 315–320, 1976.

[108] K. Mizushima, P. Jones, P. Wiseman, and J. Goodenough, "Li_xCoO_2 ($0 \leq x \leq 1$): A new cathode material for batteries of high energy density," *Materials Research Bulletin*, vol. 15, no. 6, pp. 783 – 789, 1980.

[109] H. D. Abruña, Y. Kiya, and J. C. Henderson, "Batteries and electrochemical capacitors," *Physics Today*, vol. 61, no. 12, pp. 43–47, 2008.

[110] J. Xiao, N. A. Chernova, and M. S. Whittingham, "Layered Mixed Transition Metal Oxide Cathodes with Reduced Cobalt Content for Lithium Ion Batteries," *Chemistry of Materials*, vol. 20, no. 24, pp. 7454–7464, 2008.

[111] J. B. Goodenough, "An interpretation of the magnetic properties of the perovskite-type mixed crystals $La_{1-x}Sr_xCoO_{3-\lambda}$," *Journal of Physics and Chemistry of Solids*, vol. 6, no. 2-3, pp. 287 – 297, 1958.

[112] H. M. Hollmark, L.-C. Duda, M. Dahbi, I. Saadoune, T. Gustafsson, and K. Edström, "Resonant Soft X-Ray Emission Spectroscopy and X-Ray Absorption Spectroscopy on the Cathode Material $LiNi_{0.65}Co_{0.25}Mn_{0.1}O_2$," *Journal of The Electrochemical Society*, vol. 157, no. 8, pp. A962–A966, 2010.

[113] J. Rodriguez-Carvajal, "http://www-llb.cea.fr/fullweb/powder.html."

[114] D. Sherrington and S. Kirkpatrick, "Solvable Model of a Spin-Glass," *Physical Review Letters*, vol. 35, pp. 1792–1796, Dec 1975.

[115] Laboratoire Léon Brillouin, *G4.1 diffractometer (wavelength 2.4226 Å)*.

[116] M. H. Phan, N. A. Frey, H. Srikanth, M. Angst, B. C. Sales, and D. Mandrus, "Magnetism and cluster glass dynamics in geometrically frustrated $LuFe_2O_4$," *Journal of Applied Physics*, vol. 105, no. 7, p. 07E308, 2009.

[117] H. Kobayashi, H. Sakaebe, H. Kageyama, K. Tatsumi, Y. Arachi, and T. Kamiyama, "Changes in the structure and physical properties of the solid solution $LiNi_{1-x}Mn_xO_2$ with variation in its composition," *Journal of Materials Chemistry*, vol. 13, no. 3, pp. 590–595, 2003.

[118] S. Mukherjee, R. Ranganathan, P. S. Anilkumar, and P. A. Joy, "Static and dynamic response of cluster glass in $La_{0.5}Sr_{0.5}CoO_3$," *Physical Review B*, vol. 54, pp. 9267–9274, Oct 1996.

[119] K. Jonason, J. Mattsson, and P. Nordblad, "Dynamic susceptibility of a reentrant ferromagnet," *Physical Review B*, vol. 53, pp. 6507–6513, Mar 1996.

[120] J. Magnusson, C. Djurberg, P. Granberg, and P. Nordblad, "A low field superconducting quantum interference device magnetometer for dynamic measurements," *Review of Scientific Instruments*, vol. 68, no. 10, pp. 3761–3765, 1997.

[121] D. N. H. Nam, K. Jonason, P. Nordblad, N. V. Khiem, and N. X. Phuc, "Coexistence of ferromagnetic and glassy behavior in the $La_{0.5}Sr_{0.5}CoO_3$ perovskite compound," *Physical Review B*, vol. 59, pp. 4189–4194, Feb 1999.

[122] A. G. Schins, E. M. Dons, A. F. M. Arts, H. W. de Wijn, E. Vincent, L. Leylekian, and J. Hammann, "Aging in two-dimensional Ising spin glasses," *Physical Review B*, vol. 48, pp. 16524–16532, Dec 1993.

[123] K. Jonason, J. Mattsson, and P. Nordblad, "Chaos in the Ferromagnetic Phase of a Reentrant Ferromagnet," *Physical Review Letters*, vol. 77, pp. 2562–2565, Sep 1996.

[124] S. Niidera and F. Matsubara, "Fluctuating clusters in a reentrant spin-glass system," *Physical Review B*, vol. 75, p. 144413, Apr 2007.

[125] S. Mukherjee, R. Ranganathan, and S. B. Roy, "Linear and nonlinear ac susceptibility of the canted-spin system: Ce$(Fe_{0.96}Al_{0.04})_2$," *Physical Review B*, vol. 50, pp. 1084–1089, Jul 1994.

[126] M. Suzuki, "Phenomenological Theory of Spin-Glasses and Some Rigorous Results," *Progress of Theoretical Physics*, vol. 58, no. 4, pp. 1151–1165, 1977.

[127] A. Chakravarti, R. Ranganathan, and C. Bansal, "Linear and non-linear ac susceptibility of reentrant spin glass system," *Solid State Communications*, vol. 82, no. 8, pp. 591 – 595, 1992.

[128] J. Sugiyama, H. Nozaki, Y. Ikedo, K. Mukai, P. L. Russo, D. Andreica, A. Amato, H. Yoshida, and Z. Hiroi, "Static magnetic order in metallic triangular antiferromagnet Ag_2MnO_2 detected by muon-spin spectroscopy," *Physical Review B*, vol. 78, p. 104427, Sep 2008.

Acta Universitatis Upsaliensis

Digital Comprehensive Summaries of Uppsala Dissertations from the Faculty of Science and Technology 720

Editor: The Dean of the Faculty of Science and Technology

A doctoral dissertation from the Faculty of Science and Technology, Uppsala University, is usually a summary of a number of papers. A few copies of the complete dissertation are kept at major Swedish research libraries, while the summary alone is distributed internationally through the series Digital Comprehensive Summaries of Uppsala Dissertations from the Faculty of Science and Technology. (Prior to January, 2005, the series was published under the title "Comprehensive Summaries of Uppsala Dissertations from the Faculty of Science and Technology".)

Distribution: publications.uu.se
urn:nbn:se:uu:diva-133257

ACTA
UNIVERSITATIS
UPSALIENSIS
UPPSALA
2010